RESEARCH ADVANCE

The Na^+/K^+ pump dominates control of glycolysis in hippocampal dentate granule cells

Dylan J Meyer, Carlos Manlio Díaz-García†, Nidhi Nathwani, Mahia Rahman, Gary Yellen*

Department of Neurobiology, Harvard Medical School, Boston, United States

Abstract Cellular ATP that is consumed to perform energetically expensive tasks must be replenished by new ATP through the activation of metabolism. Neuronal stimulation, an energetically demanding process, transiently activates aerobic glycolysis, but the precise mechanism underlying this glycolysis activation has not been determined. We previously showed that neuronal glycolysis is correlated with Ca^{2+} influx, but is not activated by feedforward Ca^{2+} signaling (Díaz-García et al., 2021a). Since ATP-powered Na^+ and Ca^{2+} pumping activities are increased following stimulation to restore ion gradients and are estimated to consume most neuronal ATP, we aimed to determine if they are coupled to neuronal glycolysis activation. By using two-photon imaging of fluorescent biosensors and dyes in dentate granule cell somas of acute mouse hippocampal slices, we observed that production of cytoplasmic NADH, a byproduct of glycolysis, is strongly coupled to changes in intracellular Na^+, while intracellular Ca^{2+} could only increase NADH production if both forward Na^+/Ca^{2+} exchange and Na^+/K^+ pump activity were intact. Additionally, antidromic stimulation-induced intracellular [Na^+] increases were reduced >50% by blocking Ca^{2+} entry. These results indicate that neuronal glycolysis activation is predominantly a response to an increase in activity of the Na^+/K^+ pump, which is strongly potentiated by Na^+ influx through the Na^+/Ca^{2+} exchanger during extrusion of Ca^{2+} following stimulation.

Editor's evaluation

The authors investigate mechanisms that regulate glycolytic ATP production in neurons. They conclude that the cytosolic Na^+, not Ca^{2+}, and the activity of the Na^+/K^+ pump drive glycolysis. The study is conceptually significant as it seeks to determine how neuronal glycolysis is coupled to electrical activity. The study is thoughtful, uses sophisticated fluorescence lifetime imaging technology and clever experimental designs, and as such provides new insights into how electrical activity regulates glycolysis.

***For correspondence:** gary_yellen@hms.harvard.edu

Present address: †Department of Biochemistry and Molecular Biology, University of Oklahoma Health Sciences Center, Oklahoma City, United States

Competing interest: See page 20

Funding: See page 20

Preprinted: 09 July 2022
Received: 07 July 2022
Accepted: 11 October 2022
Published: 12 October 2022

Reviewing Editor: Mark T Nelson, University of Vermont, United States

Introduction

Cellular energy consumption must be balanced by new energy production through the activation of metabolism. In neurons, energy consumption is strongest following excitation (***Attwell and Iadecola, 2002***; ***Attwell and Laughlin, 2001***; ***Engl and Attwell, 2015***; ***Howarth et al., 2012***; ***Lennie, 2003***; ***Yu et al., 2018***). Accordingly, neuronal excitation triggers a transient activation of glycolysis, which is measured as an increase to neuronal cytoplasmic NADH:NAD^+ ($NADH_{CYT}$) that can last for several minutes after the excitatory event (***Díaz-García et al., 2017***; ***Díaz-García et al., 2021a***). The specific mechanism that drives neuronal glycolysis activation has not been identified.

It seems highly plausible that glycolysis activation in neurons could be driven primarily by an increase in the activity of ion-ATPases, the ATP-powered ion transporters that move ions against their electrochemical gradients by (through a series of reaction steps; ***Post et al., 1965***; ***Sen and Post, 1964***) converting ATP into ADP and P_i (***Biondo et al., 2021***; ***Calì et al., 2018***; ***Chemaly et al., 2018***; ***Kaplan, 2002***). Ion-ATPases are estimated to be responsible for most of the energy consumption associated with neuronal signaling and are closely coupled to glycolytic enzymes across many cell types (***Ames, 2000***; ***Dhar-Chowdhury et al., 2007***; ***Dzeja and Terzic, 2003***; ***Xu et al., 1995***). Moreover, activation of glycolysis by increased ion-ATPase activity could be multimodal: a decrease to cellular ATP would stimulate glycolysis by mass action at the ATP-generating steps, while an increase to cellular ADP and P_i would stimulate glycolysis by allosterically activating phosphofructokinase and by mass action at both the glyceraldehyde-3-phosphate dehydrogenase/phosphoglycerate kinase enzyme complex and pyruvate kinase steps (***Fothergill-Gilmore and Michels, 1993***; ***Kemp and Foe, 1983***; ***Nelson et al., 2008***; ***Schöneberg et al., 2013***; ***Tomokuni et al., 2010***).

There are several ion-ATPases (also called ion pumps) that regulate neuronal Na^+ and Ca^{2+} changes (***Figure 1A***). Na^+ is handled exclusively by the Na^+/K^+-ATPase (or Na^+/K^+ pump), which uses 1 ATP molecule to export 3 Na^+ and import 2 K^+ across the plasma membrane. Ca^{2+} is handled by a diverse set of active transporters, including the plasma membrane Ca^{2+}-ATPase (PMCA), which exports 1 Ca^{2+} across the plasma membrane per ATP (***Niggli et al., 1982***; ***Thomas, 2009***), and the sarco-/endoplasmic reticulum Ca^{2+}-ATPase (SERCA), which pumps 2 Ca^{2+} into the endoplasmic reticulum lumen per ATP (***Tran et al., 2009***). Aside from ATPases, Ca^{2+} is also regulated by the Na^+/Ca^{2+}-exchanger (NCX) (***Lee et al., 2009***), a secondary active transporter that uses the electrochemical energy stored in the plasma membrane Na^+ gradient (built by the Na^+/K^+ pump) to actively export 1 Ca^{2+} by importing 3 Na^+. Any increase to neuronal Na^+ or Ca^{2+} will increase the activity of their respective ion transporters.

Transient increases to neuronal cytoplasmic Ca^{2+} (Ca^{2+}_{CYT}) induced by excitation are positively correlated with transient increases in subsequent $NADH_{CYT}$ production (***Díaz-García et al., 2017***; ***Díaz-García et al., 2021a***); in other words, stronger stimulations evoke larger increases to both Ca^{2+}_{CYT} and $NADH_{CYT}$. At first glance, this positive correlation could be (mis)interpreted as glycolysis being driven primarily by an increase in the activities of Ca^{2+} pumps (PMCA and SERCA) as Ca^{2+} is pumped from the cytoplasm. However, this readout of neuronal $NADH_{CYT}$ and Ca^{2+}_{CYT} lacks information about stimulation-induced increases to intracellular Na^+, which also likely covary with stimulation strength, so a contribution of increased Na^+/K^+ pump activity to glycolysis activation cannot be excluded.

The Na^+/K^+ pump is primed to be the predominant driving force underlying neuronal glycolysis activation. Many reports estimate that the Na^+/K^+ pump consumes ~50% of total brain energy (***Ames, 2000***; ***Astrup et al., 1981***; ***Engl and Attwell, 2015***; ***Milligan and McBride, 1985***; ***Whittam, 1962***) and uses substantially more ATP than Ca^{2+} pumps both during neurotransmission and at rest (***Attwell and Laughlin, 2001***; ***Harris et al., 2012***; ***Rolfe and Brown, 1997***). Furthermore, since Ca^{2+}_{CYT} regulation in some neurons depends strongly on the NCX (***Lee et al., 2009***), a transient Ca^{2+}_{CYT} increase could indirectly elevate intracellular [Na^+], which would potentiate any increase in Na^+/K^+ pump activity due to channel-mediated Na^+ entry.

To shed light on the mechanism of neuronal glycolysis activation, we investigated the coupling of Na^+/K^+ pump and Ca^{2+} pump activities to $NADH_{CYT}$ production in the somas of hippocampal dentate granule cells (DGCs) within acute brain slices by using two-photon fluorescence imaging of genetically encoded fluorescent biosensors and fluorescent dyes. The data provide compelling evidence indicating that increased activity of the Na^+/K^+ pump is the predominant driver of neuronal glycolysis activation, whereas increased activities of Ca^{2+} pumps appear to be negligibly coupled to glycolysis.

Results

Cytoplasmic NADH production is strongly influenced by Na^+, but not Ca^{2+}

We simultaneously monitored changes in neuronal metabolism and ion fluxes in DGC somas by expressing Peredox and RCaMP, two genetically encoded fluorescent biosensors that report NADH:NAD^+ ($NADH_{CYT}$) and free [Ca^{2+}], respectively (***Akerboom et al., 2013***; ***Hung et al., 2011***; ***Mongeon et al., 2016***). Analyte binding to Peredox (NADH in competition with NAD^+) or RCaMP (Ca^{2+}) alters each sensor's fluorescence lifetime (LT), the average time that the fluorophore spends

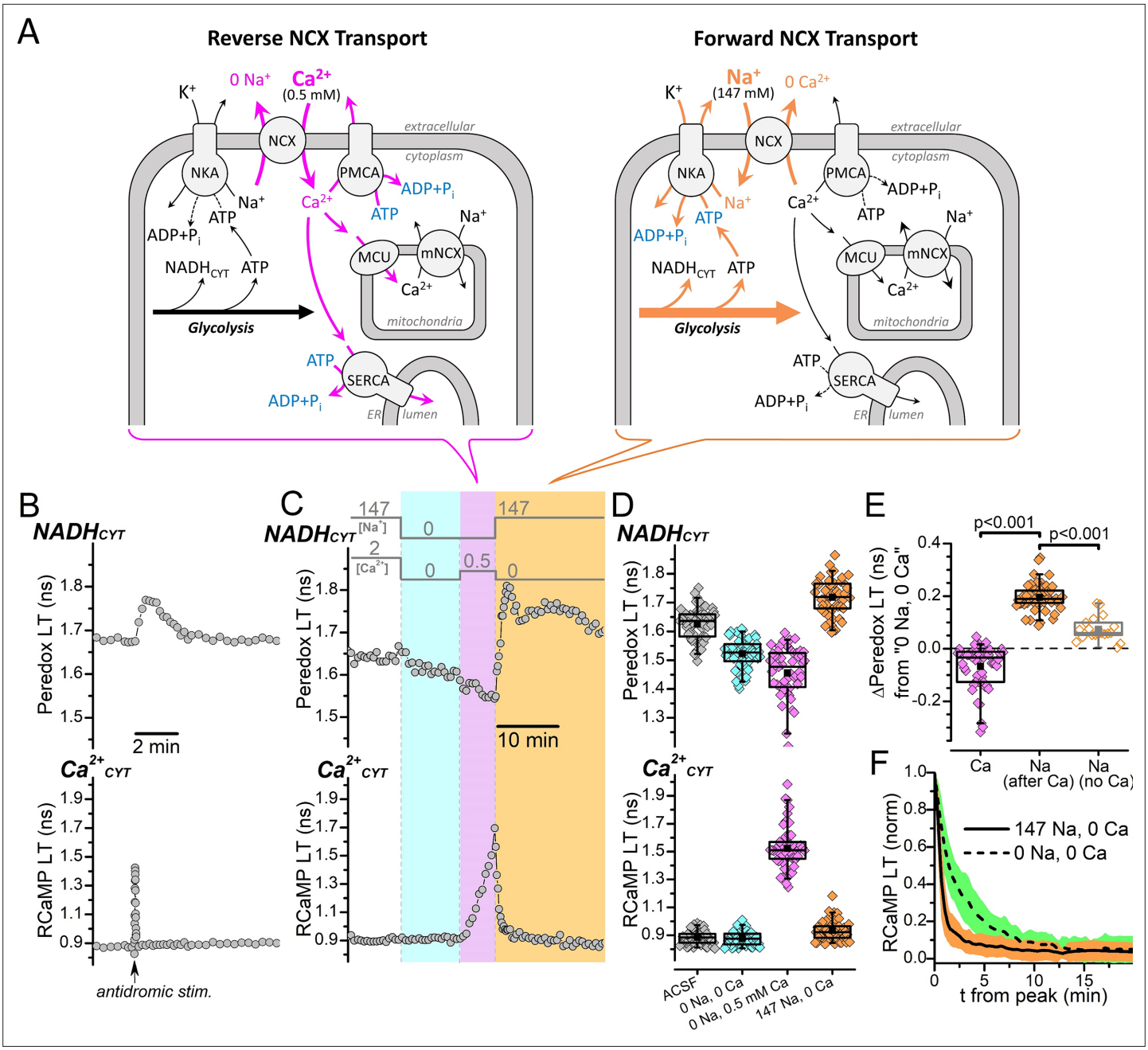

Figure 1. $NADH_{CYT}$ production is strongly influenced by Na^+, but not by $Ca^{2+}{}_{CYT}$. (**A**) Cartoon showing the NCX transport modes activated by different external [Na^+] and [Ca^{2+}] conditions and their expected effects on the activities of ion pumps and the production of $NADH_{CYT}$ from glycolysis activation. Reverse NCX transport (*left schematic*) increases intracellular [Ca^{2+}], which increases the activities Ca^{2+} pumps and Ca^{2+} transport into mitochondria (*magenta arrows*). Forward NCX transport (*right schematic*) increases intracellular [Na^+], which increases the activity of the Na^+/K^+ pump (*orange arrows*). The bracket below each schematic indicates the NCX transport mode activated by the external solution changes in (**C**). Transport stoichiometries are not indicated. Abbreviations: Na^+/Ca^{2+}-exchanger (NCX), Na^+/K^+-ATPase (NKA), plasma membrane Ca^{2+}-ATPase (PMCA), sarco-/endo-plasmic reticulum Ca^{2+}-ATPase (SERCA), mitochondrial Ca^{2+} uniporter (MCU), mitochondrial Na^+/Ca^{2+}-exchanger (mNCX), endoplasmic reticulum (ER). (**B**) Representative fluorescence lifetime (LT) traces of Peredox (*top trace*) and RCaMP (*bottom trace*) from a DGC bathed in ACSF. Antidromic stimulation was delivered at the time point indicated by the arrow along the RCaMP trace, which transiently increases both $NADH_{CYT}$ and $Ca^{2+}{}_{CYT}$. (**C**) Fluorescence LT traces of Peredox (*top*) and RCaMP (*bottom*) from a DGC showing how external Na^+ and Ca^{2+} changes affect $NADH_{CYT}$ and $Ca^{2+}{}_{CYT}$. The bars above the Peredox trace indicate the external [Na^+] and [Ca^{2+}]. $NADH_{CYT}$ was decreased by switching the bath solution from ACSF (147 mM Na^+ and 2 mM Ca^{2+}) to a solution with nominally 0 Na^+ and 0 Ca^{2+} (*cyan shading*). $Ca^{2+}{}_{CYT}$ was elevated by applying 0.5 mM Ca^{2+} with 0 Na^+ to activate reverse NCX transport (*magenta shading*), and $NADH_{CYT}$ decreased further. $NADH_{CYT}$ was strongly increased after activating forward NCX transport by the subsequent removal of external Ca^{2+} and application of 147 mM Na^+ (*orange shading*). (**D**) Box plots of the fluorescence LTs of Peredox (*top*) and RCaMP (*bottom*) showing

Figure 1 continued on next page

Figure 1 continued

the effects of the external Na^+ and Ca^{2+} changes performed in panel C across many DGCs (n=53). The external bath conditions for each box plot are listed at the bottom of the RCaMP plot in chronological order from left to right. The colors of each box plot correspond to the colors indicated in (**C**). The mean Peredox LT values in each condition were: 1.63±0.06 ns in ACSF, 1.52±0.05 ns in 0 Na^+ and 0 Ca^{2+}, 1.46±0.09 ns in 0 Na and 0.5 mM Ca^{2+}, and 1.72±0.06 ns in 147 mM Na^+ and 0 Ca^{2+}. The mean RCaMP LT values in each condition were: 0.88±0.05 ns in ACSF, 0.88±0.05 ns in 0 Na^+ and 0 Ca^{2+}, 1.52±0.15 ns in 0 Na^+ and 0.5 mM Ca^{2+}, and 0.93±0.07 ns in 147 mM Na^+ and 0 Ca^{2+}. (**E**) Changes to the Peredox LT relative to the 0 Na^+ and 0 Ca^{2+} condition, after either a Ca^{2+}_{CYT} elevation from reverse NCX transport (Ca, black box, magenta filled diamonds), an influx of Na^+ due to forward NCX transport (Na after Ca, black box, orange filled diamonds), or application of Na^+ without forward NCX (Na no Ca, gray box, orange open diamonds). The mean Peredox LT changes were: –0.07±0.08 ns (n=53) for Ca^{2+}_{CYT} elevation, 0.20±0.05 ns (n=53) for Na^+ influx via forward NCX, and 0.07364±0.04565 ns (n=19) for Na^+ application without forward NCX. Statistical significance between 'Ca' and 'Na after Ca' is indicated by a paired Wilcoxon test and between 'Na after Ca' and 'Na no Ca' by a Mann-Whitney test. (**F**) Effect of external Na^+ on the return of Ca^{2+}_{CYT} to baseline following a reverse NCX transport-mediated Ca^{2+} influx. The mean decay of the RCaMP LT following the Ca^{2+}_{CYT} increase (normalized to the peak RCaMP LT value) is shown when the external solution contained either 147 mM Na^+ (*solid line, orange SD shading*, n=53) or 0 Na^+ (*dashed line, green SD shading*, n=49). Decay data in 147 mM Na^+ were from the same DGCs as in (**D**) and (**E**), while data in 0 Na^+ were from the same DGCs as ***Figure 1—figure supplement 1B***; a representative trace of this experiment is shown in ***Figure 1—figure supplement 1A***.

The online version of this article includes the following source data and figure supplement(s) for figure 1:

Figure supplement 1. $NADH_{CYT}$ production does not increase following external Ca^{2+} removal if external Na^+ is absent.

Figure supplement 1—source data 1. The mean Peredox and RCaMP lifetimes in each external condition for ***Figure 1—figure supplement 1B***.

Figure supplement 2. Effect of thapsigargin on antidromic stimulation-induced $NADH_{CYT}$ and Ca^{2+}_{CYT} transients.

Figure supplement 3. Ca^{2+} entry from reverse NCX transport increases Ca^{2+}_{MITO}, which depends on Na^+ for removal.

Figure supplement 3—source data 1. The mean Peredox and RCaMP lifetimes in each external condition for ***Figure 1—figure supplement 3B***.

in the excited state prior to its return to the ground state (***Lakowicz, 2006***). The fluorescence LTs of Peredox and RCaMP are increased (i.e., extended in average duration) by $NADH_{CYT}$ or Ca^{2+}_{CYT} increases, respectively.

Our previous observations demonstrated that $NADH_{CYT}$ increases are strongly tied to glycolysis (***Díaz-García et al., 2017***; ***Díaz-García et al., 2021a***) and occur regardless of changes in mitochondrial metabolism: electrical-stimulation-induced increases to $NADH_{CYT}$ were substantially diminished by iodoacetic acid (an inhibitor of GAPDH) but not by AOA (an inhibitor of MAS) and were not affected by impaired NADH production in mitochondria (i.e., in the presence of inhibitors of both the mitochondrial pyruvate carrier and lactate dehydrogenase; Figure 2D in ***Díaz-García et al., 2021a***). Thus, acute $NADH_{CYT}$ changes arise directly from changes in glycolytic flux and are not strongly influenced by changes in NADH consumption by the mitochondria.

We began our investigations on the coupling of the Na^+/K^+ pump or Ca^{2+} pumps to glycolysis activation by recapitulating our previous findings: that electrical stimulation of DGCs transiently increases their $NADH_{CYT}$ production (***Díaz-García et al., 2017***; ***Díaz-García et al., 2021a***). Representative LT traces of Peredox and RCaMP, when both sensors were expressed in the cytoplasm of a DGC within a hippocampal slice that was bathed in ACSF (***Figure 1B***), show that an antidromic stimulation event delivered from an electrode placed in the hippocampal hilus causes both a fast transient increase of the RCaMP LT, reflecting a transient increase to Ca^{2+}_{CYT}, and a slower, longer-lasting transient increase of the Peredox LT, reflecting transient overproduction of $NADH_{CYT}$ by glycolysis. But since neuronal stimulation triggers influxes of both Na^+ and Ca^{2+}, the glycolysis activation could result from increases to both Na^+/K^+ pump and Ca^{2+} pump activities.

To differentiate how changes in the activities of the Na^+/K^+ pump or Ca^{2+} pumps affect glycolysis, we measured how $NADH_{CYT}$ production is affected by separate elevations of either intracellular Na^+ or Ca^{2+}_{CYT} (***Figure 1C***). If glycolysis is preferentially coupled to the activity of either the Na^+/K^+ pump or Ca^{2+} pumps, then $NADH_{CYT}$ production should be coupled to changes in the levels of the transported ion (Na^+ or Ca^{2+}). Simultaneous removal of both Na^+ and Ca^{2+} from the bath solution (by external ion substitution) decreased the Peredox LT from its baseline in ACSF (***Figure 1C***), which indicates a decrease to $NADH_{CYT}$; we can attribute this $NADH_{CYT}$ decrease entirely to the removal of Na^+, since removing only Ca^{2+} slightly increases $NADH_{CYT}$ (cf. Figure 6—figure supplement 1b in ***Díaz-García et al., 2021a***). This $NADH_{CYT}$ decrease suggests that the rate of glycolysis can be slowed by depleting the intracellular [Na^+], which would decrease the activity of the Na^+/K^+ pump. The RCaMP LT was not affected by the removal of Na^+ and Ca^{2+} (***Figure 1C***), indicating that Ca^{2+}_{CYT} was maintained at or below resting levels, near the floor of RCaMP's dynamic range (***Akerboom et al., 2013***).

Following the removal of external Na^+ and Ca^{2+}, we added each ion back one at a time to separately increase either intracellular Na^+ or Ca^{2+}. We increased Ca^{2+} by applying 0.5 mM external Ca^{2+} in the nominal absence of external Na^+ to facilitate Ca^{2+} entry via reverse NCX transport, and the expected strong increase in Ca^{2+}_{CYT} was confirmed by an increase in the RCaMP LT (***Figure 1C***, during the magenta shaded interval). However, this increase to Ca^{2+}_{CYT} was not associated with an increase to $NADH_{CYT}$. In fact, the opposite occurred: Ca^{2+}_{CYT} elevation decreased the Peredox LT even further from the 0 Na^+ 0 Ca^{2+} bath condition (possibly due to the extrusion of Na^+ during reverse NCX; see Discussion). At this point, with Ca^{2+}_{CYT} elevated, we removed 0.5 mM external Ca^{2+} and re-applied external Na^+ to facilitate strong Na^+ influx via forward NCX transport (in exchange for Ca^{2+}_{CYT}), which promptly increased $NADH_{CYT}$. Following the external Na^+ application, Ca^{2+}_{CYT} returned to baseline levels (***Figure 1C***, orange shaded interval).

The decrease to Peredox LT by removing external Na^+ and the increase to Peredox LT from re-applying external Na^+, across many DGCs (***Figure 1D***), show that $NADH_{CYT}$ is strongly influenced by Na^+. Relative to the Peredox LT in the 0 Na^+ 0 Ca^{2+} bath condition, the Peredox LT was *decreased* when Ca^{2+}_{CYT} was elevated but *increased* following external Na^+ re-application (***Figure 1E***), which suggests that glycolysis activation is strongly tied to the activity of the Na^+/K^+ pump, but not strongly tied to the activity of Ca^{2+} pumps (nor to the increase in Ca^{2+}_{CYT} per se, e.g., via a signaling mechanism).

Our ion substitution experiments also hinted that both glycolysis activation and Ca^{2+}_{CYT} regulation in DGCs are dependent on forward NCX transport. A Ca^{2+}_{CYT} increase (from reverse NCX transport) returned faster to baseline levels if external Na^+ was present (i.e., if forward NCX was activated, ***Figure 1F***; and compare ***Figure 1C*** with ***Figure 1—figure supplement 1A***), and $NADH_{CYT}$ did not increase following a Ca^{2+}_{CYT} increase if external Ca^{2+} was removed without re-applying external Na^+ (***Figure 1—figure supplement 1A and B***). $NADH_{CYT}$ production increased when external Na^+ was removed and re-applied without previously elevating Ca^{2+}_{CYT} (i.e., without activating forward NCX, ***Figure 1—figure supplement 1C and D***), but this $NADH_{CYT}$ increase was weaker than when external Na^+ was re-applied while Ca^{2+}_{CYT} was elevated (i.e., when forward NCX was activated, ***Figure 1D and E***).

The inability of a Ca^{2+}_{CYT} elevation to measurably stimulate $NADH_{CYT}$ production in the absence of external Na^+ suggests that any increase in activity of PMCA and SERCA to pump Ca^{2+} from the cytoplasm does not substantially activate glycolysis, even during the prolonged Ca^{2+}_{CYT} increases in our ion substitution experiments. But maybe inhibiting one of these Ca^{2+} pumps, to divert more Ca^{2+}_{CYT} to be extruded by the non-inhibited pump, could boost the activity of the other and consequently amplify its associated effect on glycolysis. We tested this possibility by inhibiting SERCA, which compared to PMCA has more specific pharmacology and uses less ATP per Ca^{2+} transported. Thapsigargin (1 μM, a specific SERCA inhibitor) increased both the $NADH_{CYT}$ and Ca^{2+}_{CYT} transients evoked by antidromic electrical stimulations in ACSF (***Figure 1—figure supplement 2A and B***) as well as the ΔPeredox/ΔR-CaMP ratio (***Figure 1—figure supplement 2C***). These effects are consistent with SERCA inhibition and a diversion of Ca^{2+}_{CYT} to other clearance pathways that are either more closely coupled to glycolysis or that transport fewer ions per ATP utilized. However, reverse-NCX-mediated Ca^{2+}_{CYT} increases in the presence of 1 μM thapsigargin (and absence of external Na^+) still failed to increase $NADH_{CYT}$ (***Figure 1—figure supplement 1B***), meaning that any putative amplification of PMCA activity after SERCA inhibition was still not enough to drive measurable glycolysis activation.

We have previously shown that electrical stimulation increases DGC mitochondrial Ca^{2+} (Ca^{2+}_{MITO}) from Ca^{2+} entry through the mitochondrial Ca^{2+} uniporter (MCU) (***Díaz-García et al., 2021a***). Could Ca^{2+}_{CYT}'s failure to activate $NADH_{CYT}$ production during our ion substitution experiments be due to a lack of activation of some unknown Ca^{2+}_{MITO}-dependent process? This seems unlikely, as bath-applied 0.5 mM external Ca^{2+} in the absence of external Na^+ increased the fluorescence LT of mitochondrially targeted RCaMP (***Figure 1—figure supplement 3A and B***), indicating that Ca^{2+}_{MITO} is increased by reverse-NCX-mediated Ca^{2+} entry. Ca^{2+}_{MITO} slightly decreased when external Ca^{2+} was removed, but complete return of Ca^{2+}_{MITO} to baseline levels was not achieved until external Na^+ was applied, demonstrating that Ca^{2+}_{MITO} regulation is dependent on Na^+, like Ca^{2+}_{CYT}.

In summary, these ion substitution experiments show that neuronal $NADH_{CYT}$ production is closely coupled to the flux of Na^+, and that a Ca^{2+}_{CYT} elevation is not sufficient to elevate $NADH_{CYT}$ regardless of whether it is pumped by SERCA, pumped by PMCA, or taken up into mitochondria via MCU. They also show that $NADH_{CYT}$ production is activated more strongly by conditions that favor forward

NCX transport that exchanges Ca^{2+}_{CYT} for Na^+, and that regulation of both DGC Ca^{2+}_{CYT} and Ca^{2+}_{MITO} depends on Na^+. These observations suggest that neuronal glycolysis is both strongly coupled to the activity of the Na^+/K^+ pump and sensitive to Na^+ import via forward NCX transport, which would become activated following an excitatory event where Ca^{2+}_{CYT} must be removed.

Malate-aspartate shuttle activity does not mask a Ca^{2+}-induced increase to $NADH_{CYT}$

The malate-aspartate shuttle (MAS) is a major pathway that recycles $NADH_{CYT}$ by transferring reducing equivalents from $NADH_{CYT}$ to mitochondria (***McKenna et al., 2006***; ***Satrústegui and Bak, 2015***). MAS activity is activated by Ca^{2+}_{CYT} elevations but is reduced by Ca^{2+}_{MITO} elevations (***Contreras and Satrústegui, 2009***; ***Satrústegui and Bak, 2015***), which likely means that neuronal excitation would cause a brief MAS activation followed by a longer inhibition, mirroring the Ca^{2+}_{CYT} and Ca^{2+}_{MITO} transient time courses (***Contreras and Satrústegui, 2009***). But the state of MAS activity in our ion substitution experiments was uncertain since reverse NCX transport produced prolonged increases to both Ca^{2+}_{CYT} and Ca^{2+}_{MITO} (***Figure 1*** and ***Figure 1—figure supplement 3***), so it remained a possibility that

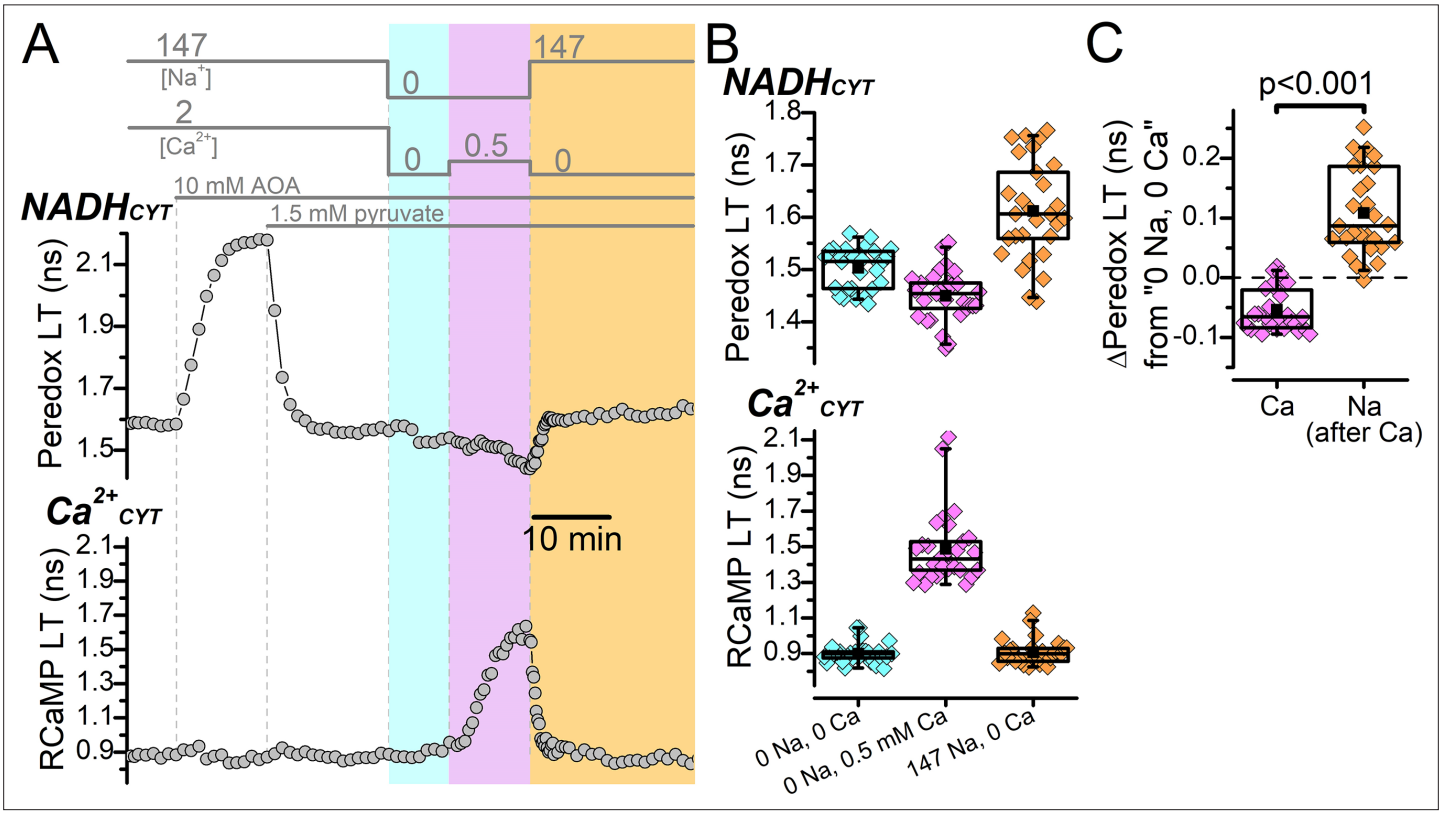

Figure 2. Malate-aspartate shuttle activity does not conceal a possible $NADH_{CYT}$ increase produced by elevated Ca^{2+}_{CYT}. (**A**) Representative fluorescence lifetime (LT) traces of Peredox (*top*) and RCaMP (*bottom*) from a DGC. External solution changes are indicated by the bars above the Peredox trace. The recording begins in ACSF (147 mM Na^+ and 2 mM Ca^{2+}), where the addition of 10 mM AOA strongly increases the Peredox LT. Addition of 1.5 mM pyruvate reverted the Peredox LT approximately back to baseline. Following this, external Na^+ and Ca^{2+} were removed (*cyan shading*), which slightly decreased the Peredox LT. The addition of 0.5 mM Ca^{2+} in 0 Na^+ to stimulate reverse NCX transport increased the RCaMP LT and further decreased the Peredox LT (*magenta shading*). Subsequently, the removal of external Ca^{2+} and re-addition of external Na^+ to stimulate forward NCX transport (*orange shading*) increased the Peredox LT and brought the RCaMP LT back to baseline. (**B**) Box plots of the Peredox (*top*) and RCaMP (*bottom*) fluorescence LTs in the different external solution conditions performed in (**A**), across many DGCs (n=29). The external [Na^+] and [Ca^{2+}] condition after applying AOA and pyruvate is listed across the bottom in chronological order from left to right. The coloring of the data corresponds to the shading in A. The mean Peredox and RCaMP LTs in each external condition were (in ns): 1.50±0.04 in 0 Na^+ and 0 Ca^{2+}, 1.45±0.05 in 0 Na^+ and 0.5 mM Ca^{2+}, and 1.61±0.09 in 147 Na^+ and 0 Ca^{2+}. The mean RCaMP LTs were (in ns): 0.90±0.06 in 0 Na^+ and 0 Ca^{2+}, 1.49±0.20 in 0 Na^+ and 0.5 mM Ca^{2+}, and 0.91±0.07 in 147 Na^+ and 0 Ca^{2+}. (**C**) Relative change to the Peredox fluorescence LT induced by the addition of 0.5 mM Ca^{2+} in the absence of external Na^+ to stimulate reverse NCX transport (Ca) or 147 mM Na^+ in the absence of external Ca^{2+} to stimulate forward NCX transport (Na). The data are from the same DGCs as in (**B**). The mean ΔPeredox values were: –0.05±0.04 ns for 'Ca' and 0.11±0.07 ns for 'Na'. Statistical significance from a paired Wilcoxon test is indicated.

Ca^{2+}_{CYT} activation of MAS could increase $NADH_{CYT}$ recycling and conceal any small increase to $NADH_{CYT}$ production due to increased activity of Ca^{2+} pumps. Therefore, we tested if a Ca^{2+}_{CYT} elevation could increase $NADH_{CYT}$ after MAS inhibition (***Figure 2***).

Representative fluorescence LT traces from a DGC show that Peredox LT was substantially increased by the application of AOA to block the shuttle's aspartate aminotransferase enzyme (***Figure 2A***), as previously described, ***Díaz-García et al., 2017***, which is consistent with an inhibition of $NADH_{CYT}$ recycling and consequent elevation of the cytoplasmic NADH:NAD^+. This strong increase to Peredox LT, which approaches the upper end of its dynamic range, precludes the ability to measure further $NADH_{CYT}$ increases, so we applied exogenous pyruvate (1.5 mM) to promote the oxidation of NADH to NAD^+ via lactate dehydrogenase and restore the Peredox LT approximately back to its baseline LT in ACSF. We then removed external Na^+ and Ca^{2+}, which decreased the Peredox LT from the AOA and pyruvate condition (***Figure 2A***); and then increased Ca^{2+}_{CYT} by applying 0.5 mM external Ca^{2+} in zero external Na^+ to drive reverse NCX transport. We confirmed the Ca^{2+}_{CYT} increase from the increase to RCaMP LT, but the Ca^{2+}_{CYT} elevation still did not coincide with an increase to $NADH_{CYT}$. Rather, $NADH_{CYT}$ decreased relative to the 0 Na^+ 0 Ca^{2+} baseline (***Figure 2B and C***). This demonstrates that an increase to Ca^{2+}_{CYT} still fails to observably stimulate $NADH_{CYT}$ production even when $NADH_{CYT}$ recycling by the MAS is attenuated. Following the Ca^{2+}_{CYT} increase, we removed 0.5 mM external Ca^{2+} and re-applied external Na^+ to activate forward NCX transport (***Figure 2A***), which increased the Peredox LT (***Figure 2B and C***). This shows again that $NADH_{CYT}$ production is coupled to the flux of Na^+.

Overall, these experiments argue against a concealment of Ca^{2+}_{CYT}-induced $NADH_{CYT}$ production by a Ca^{2+}_{CYT} activation of $NADH_{CYT}$ recycling via the MAS and indicates, once again, that an increase to Na^+/K^+ pump activity is the major driver of glycolysis.

Activation of glycolysis by Ca^{2+} is mediated by coupling between the Na^+/Ca^{2+}-exchanger and the Na^+/K^+ pump

The increase to $NADH_{CYT}$ production by an influx of Na^+ (***Figure 1*** and ***Figure 2***) suggests that glycolysis activation in DGCs is strongly tied to an increase in the activity of the Na^+/K^+ pump. Also, the $NADH_{CYT}$ increase induced by external Na^+ application was stronger if Ca^{2+}_{CYT} was elevated compared to when Ca^{2+}_{CYT} was *not* elevated (***Figure 1E***), meaning that forward NCX transport, which trades Ca^{2+}_{CYT} for Na^+, can potentiate glycolysis activation. By considering these observations together with the apparent insensitivity of glycolysis to increases in Ca^{2+} pump activity, it seemed logical that a transient Ca^{2+}_{CYT} elevation would activate glycolysis predominantly by stimulating Na^+ influx through forward NCX transport, which would then increase the activity of the Na^+/K^+ pump.

We sought for a way to directly test how $NADH_{CYT}$ is affected by inhibition of the Na^+/K^+ pump or inhibition of forward NCX transport (***Figure 3***). Na^+/K^+ pumps are specifically inhibited by ouabain, although the rodent Na^+/K^+ pump α1-isozymes have relatively low sensitivity and require millimolar inhibitor concentrations for complete inhibition under physiological conditions (***Blanco and Mercer, 1998***; ***Marks and Seeds, 1978***). Application of 2 mM ouabain to DGCs bathed in ACSF quickly led to Ca^{2+} overload and cell rupture (***Figure 3—figure supplement 1***), which made it impossible to measure how electrical stimulation-induced $NADH_{CYT}$ transients are affected by complete Na^+/K^+ pump inhibition. Clearly, the activity of the Na^+/K^+ pump must be substantial, even at rest, but achieving complete Na^+/K^+ pump inhibition under physiological neuronal conditions is challenging. DGCs bathed in ACSF were more tolerant to application of low-dose (5 μM) ouabain, which inhibits only the rodent Na^+/K^+ pump α2- and α3-isozymes that have higher inhibitor sensitivities (***Blanco and Mercer, 1998***), but the stimulation-induced $NADH_{CYT}$ transient was not eliminated (***Figure 3—figure supplement 2***). This result argues that in these cells, the α1 subunit is adequate to support the activation of glycolysis.

We successfully established a condition amenable to millimolar ouabain application by reducing the external [Na^+] to 40 mM and removing external Ca^{2+} to prevent unintended reverse NCX transport. Stimulation-induced Ca^{2+}_{CYT} transients using an electrode were not possible for DGCs bathed in this condition, but we evoked similar Ca^{2+}_{CYT} transients by applying puffs of extracellular Ca^{2+} to transiently produce reverse-NCX transport (***Figure 3A***). A brief puff of Ca^{2+} to a DGC within a slice bathed in 40 mM Na^+ and 0 Ca^{2+} (***Figure 3B***) induced a fast transient increase to the RCaMP LT, reflecting a fast increase to Ca^{2+}_{CYT}, followed by a transient increase to the Peredox LT, reflecting an increase to $NADH_{CYT}$. This shows that a transient Ca^{2+}_{CYT} elevation can, indeed, activate glycolysis under these ionic conditions. But for a DGC within a slice that was instead bathed in zero external Na^+ to prevent

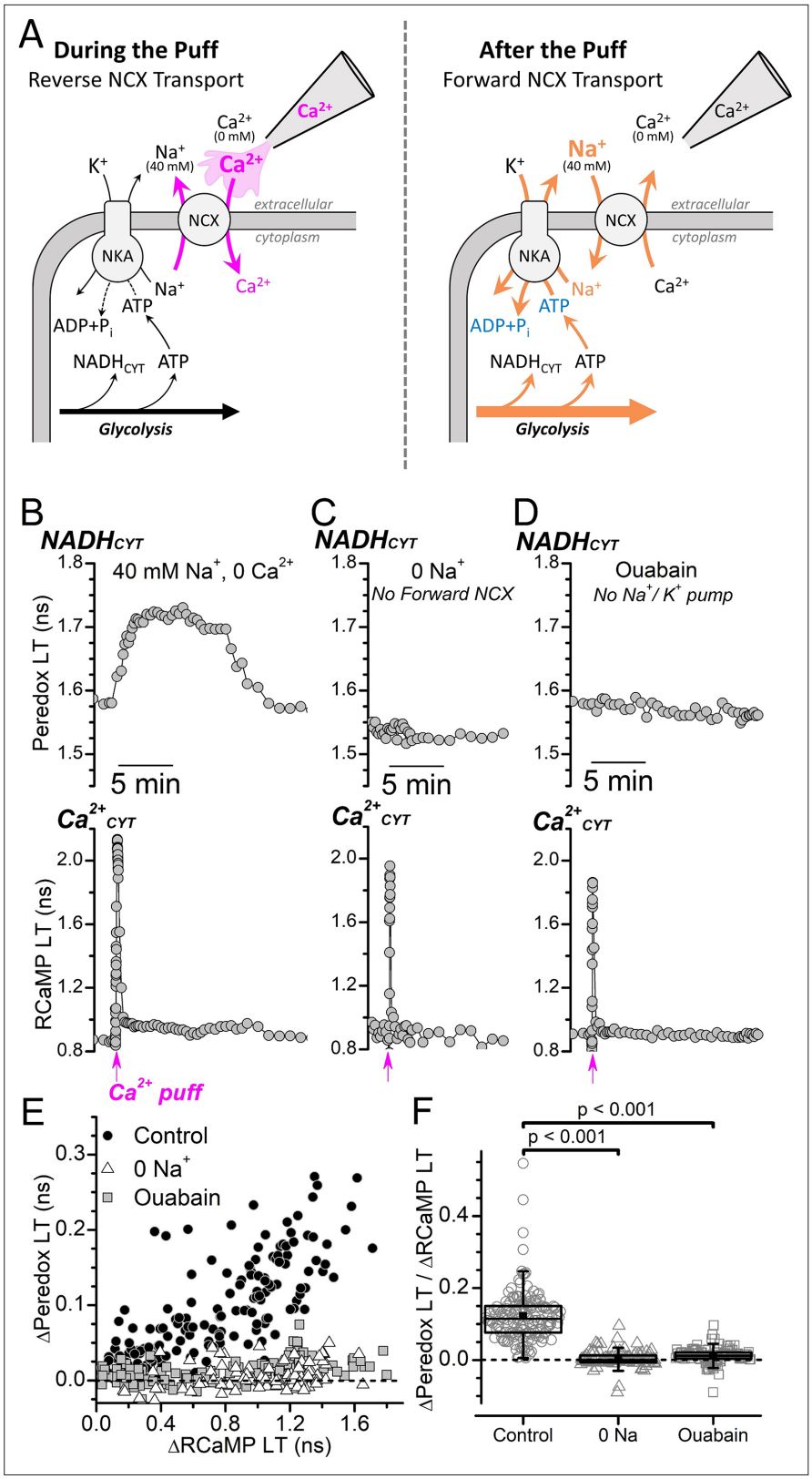

Figure 3. Ca^{2+}_{CYT} transients induced by external Ca^{2+} puffs only increase $NADH_{CYT}$ production when both forward NCX transport and Na^+/K^+ pump activity are intact. (**A**) Cartoon depicting the expected effect of a local external Ca^{2+} puff on ion transport by the NCX and subsequent activation of the Na^+/K^+ pump. (*Left*) A pipette containing Ca^{2+} is placed near the soma of a DGC within a slice that is bathed in solution containing 40 mM Na^+ and 0 Ca^{2+}

Figure 3 continued on next page

Figure 3 continued

solution. A brief pulse of positive pressure is applied to the pipette to transiently increase the local external [Ca^{2+}] and stimulate reverse NCX transport (*magenta arrows*), leading to Ca^{2+} import and an increase to Ca^{2+}_{CYT}. (*Right*) In the aftermath of the puff, the local external [Ca^{2+}] decreases as the small volume of puffed Ca^{2+} mixes with large volume of the 40 mM Na^+ 0 Ca^{2+} bath solution, which leads to forward NCX transport that stimulates Na^+ extrusion and an increase to Na^+/K^+ pump activity (*orange arrows*). Abbreviations: Na^+/Ca^{2+}-exchanger (NCX), Na^+/K^+-ATPase (NKA). (**B–D**) Representative fluorescence lifetime (LT) traces of Peredox (*top traces*) and RCaMP (*bottom traces*) from a DGC bathed in either 40 mM Na^+ and 0 Ca^{2+} solution (**B**, *Control*), 0 Na^+ and 0 Ca^{2+} to block forward NCX transport (**C**, *0 Na^+*), or in 40 mM Na^+ and 0 Ca^{2+} with 5 mM ouabain to block the Na^+/K^+ pump (**D**, *Ouabain*). Puffs of Ca^{2+} were delivered at the timepoint indicated along the bottom of the RCaMP LT traces (*magenta arrows*). (**E**) Scatterplot of the Ca^{2+}-puff-induced transient changes to the Peredox and RCaMP LTs of DGCs in 40 mM Na^+ and 0 Ca^{2+} (*Control, black circles*, n=172), in 0 Na^+ and 0 Ca^{2+} (*0 Na^+, white triangles*, n=102), or in 40 mM Na^+ and 0 Ca^{2+} with 5 mM ouabain (*Ouabain, gray squares*, n=114). The dashed line indicates where ΔPeredox=0. Analysis was restricted to recordings with transient RCaMP LT half-decay times <35 s. (**F**) Ratio of ΔPeredox to ΔRCaMP for the same Ca^{2+}-puff-induced LT transients as in panel E, except excluding those recordings where the ΔRCaMP LT was <0.2 ns to avoid noisy ratio calculations due to small ΔRCaMP values. The dashed line indicates where ΔPeredox/ΔRCaMP=0. The mean ΔPeredox/ΔRCaMP in each condition was: 0.12±0.07 in 40 mM Na^+ and 0 Ca^{2+} (*Control*, n=147), 0.01±0.02 in 0 Na^+ and 0 Ca^{2+} (*0 Na^+*, n=96), and 0.00±0.02 in 40 mM Na^+ and 0 Ca^{2+} with 5 mM ouabain (*Ouabain*, n=99). Statistical significance from Mann-Whitney tests is indicated.

The online version of this article includes the following figure supplement(s) for figure 3:

Figure supplement 1. Complete Na^+/K^+ pump inhibition in ACSF leads to cell rupture.

Figure supplement 2. Effect of low dose (5 μM) ouabain on transient Peredox and RCaMP lifetime (LT) increases evoked by synaptic or antidromic stimulation.

the NCX-mediated influx of Na^+ in exchange for the elevated Ca^{2+}_{CYT}, a Ca^{2+} puff still evoked a fast Ca^{2+}_{CYT} transient but did not increase $NADH_{CYT}$ (***Figure 3C***). Similarly, the $NADH_{CYT}$ increase that would normally follow the Ca^{2+} puff was prevented for a DGC within a slice bathed with 5 mM ouabain to block Na^+/K^+ pumps (***Figure 3D***).

A scatter plot of the transient Peredox LT and RCaMP LT changes that were evoked by Ca^{2+} puffs (***Figure 3E***) illustrates the positive correlation between $NADH_{CYT}$ production and Ca^{2+}_{CYT} increases for DGCs bathed in 40 mM Na^+ and 0 Ca^{2+}, where both forward NCX and Na^+/K^+ pump activities are intact. But $NADH_{CYT}$ production was deeply attenuated when DGCs were bathed without external Na^+ or with 5 mM ouabain, even with large elevations of Ca^{2+}_{CYT} (ΔRCaMP>1.2 ns). The mean ΔPeredox/ΔRCaMP ratio (***Figure 3F***) for Ca^{2+}-puff-evoked transients in 40 mM external Na^+ (0.122±0.005, n=147) was reduced to nearly 0 after blocking forward NCX transport by removing external Na^+ (0.003±0.002, n=96) or after blocking the Na^+/K^+ pump with ouabain (0.013±0.002, n=99).

These data demonstrate that Ca^{2+}_{CYT} can activate glycolysis in the DGC soma if it is traded for Na^+ through forward NCX transport, which increases the activity of the Na^+/K^+ pump. The lack of Ca^{2+}-puff-induced $NADH_{CYT}$ responses when either forward NCX transport or the Na^+/K^+ pump was blocked further substantiates that any increase in the activity of Ca^{2+} pumps has a negligible effect on glycolysis activation.

Antidromic stimulation-induced Na^+ transients depend on Ca^{2+}

The stimulation of $NADH_{CYT}$ production by Ca^{2+}_{CYT} through coupling between forward NCX transport and the Na^+/K^+ pump (***Figure 3***) indicates that Na^+ influx during forward NCX transport can activate glycolysis. But how does the amount of Na^+ imported by the NCX to extrude Ca^{2+}_{CYT} compare to the total Na^+ influx induced by neuronal excitation? We investigated this by measuring intracellular [Na^+] changes during electrical stimulation with and without Ca^{2+} entry (***Figure 4A***).

We recorded stimulation-induced changes in intracellular [Na^+] and Ca^{2+}_{CYT} simultaneously by loading SBFI (***Harootunian et al., 1989***), a Na^+-sensitive fluorescence dye, into RCaMP-expressing DGCs via single-cell electroporation. Representative traces of the SBFI relative fluorescence intensity (ΔF/F) and RCaMP LT from a DGC bathed in ACSF show that antidromic stimulation evoked a transient decrease to SBFI ΔF/F (note the inverted y-axis), reflecting an increase to [Na^+], and a transient increase to RCaMP LT, reflecting an increase to Ca^{2+}_{CYT} (***Figure 4B***). SBFI ΔF/F transients were longer in duration than the RCaMP LT transient, regardless of whether they were evoked by antidromic stimulation or synaptic stimulation in the absence of synaptic blockers (***Figure 4*** and ***Figure 4—figure***

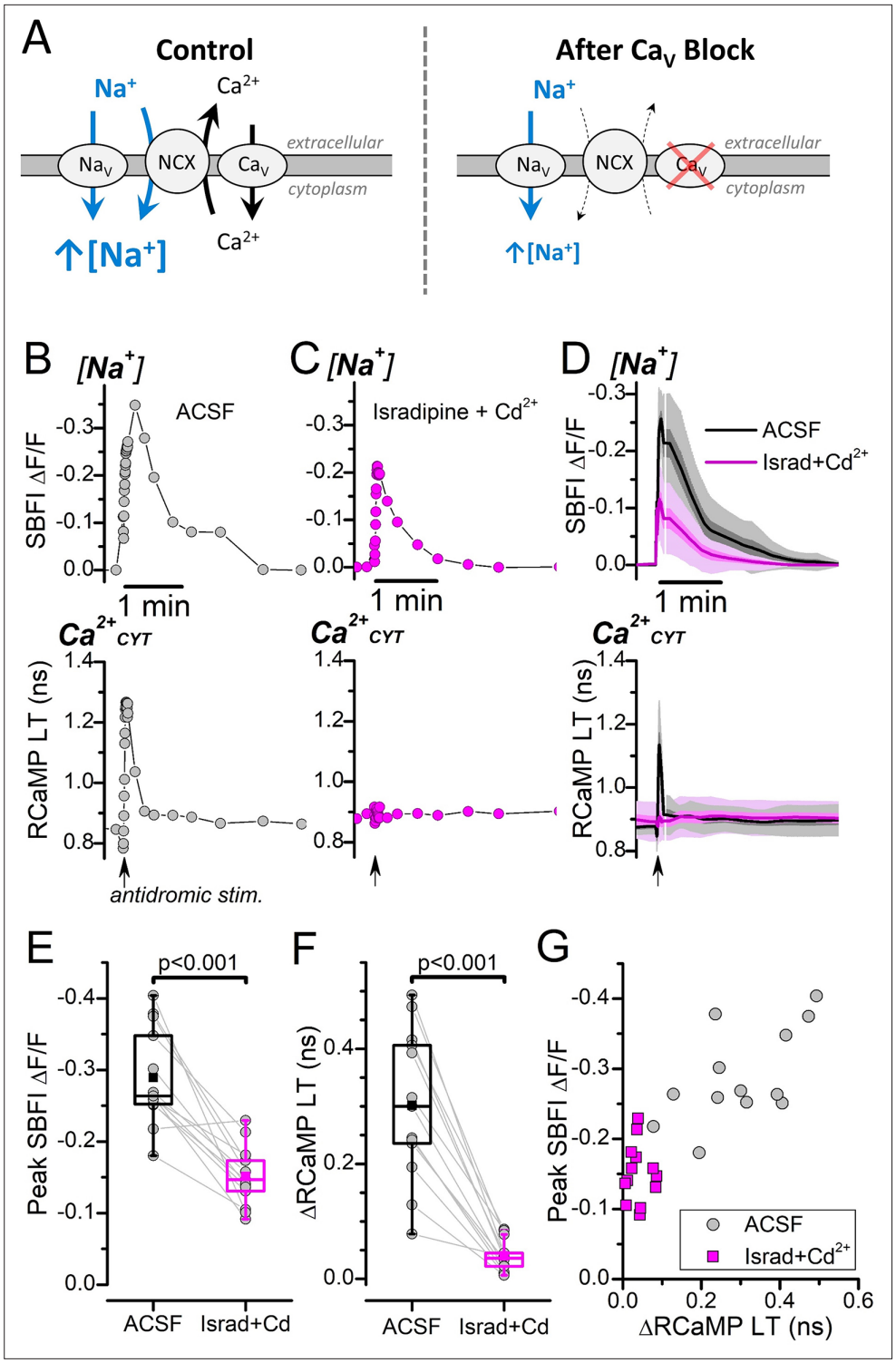

Figure 4. Antidromic stimulation-induced [Na$^+$] transients depend strongly on Ca^{2+} entry. (**A**) Cartoon depicting antidromic stimulation-induced Na$^+$ and Ca^{2+} fluxes. *Left, Control*: Stimulation in ACSF triggers Na$^+$ and Ca^{2+} influx through their respective voltage-gated Na$^+$ and Ca^{2+} channels. Following the Ca$^{2+}_{CYT}$ elevation, the NCX will import Na$^+$ to drive Ca^{2+} extrusion. Both the Na$^+$ influx through Na$_V$ and through the NCX contribute to the total intracellular [Na$^+$] increase (*blue arrows*). *Right, After Ca$_V$ Block*: Inhibiting Ca^{2+} influx through Ca$_V$ (indicated by the *red X*) prevents Ca$^{2+}_{CYT}$ elevation, which strongly reduces Na$^+$ influx through the NCX. Abbreviations: voltage-gated Na$^+$ channel (Na$_V$), voltage-gated Ca^{2+} channel (Ca$_V$), Na$^+$/Ca^{2+}-exchanger (NCX). (**B**) Representative fluorescence traces showing antidromic stimulation-induced transient changes to SBFI ΔF/F (*top*) and RCaMP lifetime (LT)

Figure 4 continued on next page

Figure 4 continued

(*bottom*) from a DGC bathed in ACSF with synaptic blockers. The stimulation was delivered at the timepoint indicated by the arrow at the bottom of the RCaMP trace. The SBFI ΔF/F axis is inverted to illustrate an increase to $[Na^+]$ as an upward deflection. (**C**) Antidromic stimulation-induced transient changes to SBFI ΔF/F and RCaMP LT in the presence of 3 μM isradipine and 20 μM $CdCl_2$ for the same DGC as in (**B**). The stimulation was delivered at the timepoint indicated by the arrow below the RCaMP trace. (**D**) Average, interpolated, antidromic stimulation-induced SBFI ΔF/F and RCaMP LT transients (n=13) before (*ACSF, black trace and shading*) and after Ca_V block (*Israd+Cd^{2+}, magenta trace and shading*). The means are indicated by the solid line, SEM is indicated by the darker shading, and SD is indicated by the lighter shading. (**E**) Paired box plots showing the antidromic stimulation-induced peak transient SBFI ΔF/F amplitudes before (*ACSF, black box*) and after Ca_V block (*Israd+Cd^{2+}, magenta box*) for the same DGCs as in (**D**). The mean peak SBFI ΔF/F values were: –0.29±0.07 in ACSF and –0.15±0.04 with Israd+Cd^{2+}. Statistical significance from a paired sample t-test is indicated. (**F**) Paired box plots showing the ΔRCaMP LT before (*ACSF, black box*) after Ca_V block (*Israd+Cd^{2+}, magenta box*) for the same DGCs as in (**D**) and (**E**). The mean ΔRCaMP LTs were: 0.30±0.13 ns in ACSF and 0.04±0.03 ns with Israd+Cd^{2+}. Statistical significance from a paired sample t-test is indicated. (**G**) Scatterplot of antidromic stimulation-induced transient changes to SBFI ΔF/F against ΔRCaMP LT before (*ACSF, gray circles*) and after Ca_V block (*Israd +Cd^{2+}, magenta squares*). Data are from the same DGCs as in (**D–F**).

The online version of this article includes the following figure supplement(s) for figure 4:

Figure supplement 1. Somatic intracellular $[Na^+]$ and Ca^{2+}_{CYT} transients induced by synaptic or antidromic stimulation.

supplement 1), indicating that stimulation-induced intracellular $[Na^+]$ elevation outlasts Ca^{2+}_{CYT} elevation. A scatterplot of the transient changes to SBFI ΔF/F and RCaMP LT shows that intracellular $[Na^+]$ and Ca^{2+}_{CYT} changes are positively correlated when evoked by either stimulation paradigm (***Figure 4—figure supplement 1D***); while this is consistent with a positive dependence of intracellular $[Na^+]$ on Ca^{2+}_{CYT}, a positive correlation between $[Na^+]$ and Ca^{2+}_{CYT} increases would also be observed if neuronal stimulation evokes proportional yet independent changes to both ions.

To directly test if somatic intracellular $[Na^+]$ changes depend on Ca^{2+} entry, we measured how antidromic stimulation-induced $[Na^+]$ transients were affected by blocking Ca^{2+} channels (***Figure 4A***). Blocking voltage-gated Ca^{2+} channels with isradipine and Cd^{2+} (***Berjukow et al., 2000***; ***Lansman et al., 1986***) attenuated the antidromic stimulation-induced RCaMP LT transient (***Figure 4C and D***), indicating a strong reduction to Ca^{2+} entry and Ca^{2+}_{CYT} elevation. The SBFI ΔF/F transient became smaller after blocking Ca^{2+} entry (***Figure 4C and D***), demonstrating that stimulation-induced intracellular $[Na^+]$ changes depend on Ca^{2+}_{CYT} elevation; the peak of the SBFI Na^+ transient (as ΔF/F) was reduced to 54.6±19.3% of the original response and the Ca^{2+} transient (as ΔRCaMP LT) was reduced to 14.5±12.5% (n=13) (***Figure 4E and F***).

A scatterplot of the antidromic stimulation-induced transient changes to SBFI ΔF/F and ΔRCaMP LT in ACSF or in the presence of isradipine and Cd^{2+} (***Figure 4G***) shows that blocking Ca^{2+} entry shifts the peak SBFI ΔF/F down and to the left, which indicates that a major component of somatic $[Na^+]$ changes is dependent on Ca^{2+}_{CYT}. This means that Na^+ imported by forward NCX transport in response to Ca^{2+}_{CYT} extrusion comprises a substantial proportion of the Na^+ that enters the soma following stimulation, which provides clarity to the apparent dependence of antidromic stimulation-induced glycolysis activation on Ca^{2+}_{CYT} elevation (***Díaz-García et al., 2021a***): an elevation to Ca^{2+}_{CYT} potentiates Na^+ influx, which ultimately leads to a stronger activation of the Na^+/K^+ pump than when Ca^{2+} entry is blocked.

Discussion

Glycolysis in neurons is transiently increased following stimulation (***Díaz-García et al., 2017***; ***Fox et al., 1988***; ***Fox and Raichle, 1986***). To understand the mechanism that drives this increase to glycolysis following neuronal electrical activity, we tested the responsiveness of $NADH_{CYT}$ to changes in intracellular Na^+ and $Ca^{2+}_{CYT,}$ which affect energy consumption by ion-ATPases. We have shown in hippocampal DGC somas that $NADH_{CYT}$ is strongly influenced by changes in intracellular Na^+ and that activation of $NADH_{CYT}$ increases by Ca^{2+}_{CYT} is nearly completely dependent on ion transport coupling between the NCX and the Na^+/K^+ pump. This means that nearly all of the transient glycolysis increase

following a stimulation is a response to an activation of the Na^+/K^+ pump to extrude the Na^+ that enters either through Na^+ channels or through the NCX to power active Ca^{2+} transport.

Neuronal glycolysis is strongly influenced by the Na^+/K^+ pump, but not by Ca^{2+} pumps

Coupling between glycolysis and Na^+/K^+ pump activity has been reported across many tissues and cell types (***Andersen and Marmarou, 1992***; ***Balaban and Bader, 1984***; ***Hasin and Barry, 1984***; ***Hellstrand et al., 1984***; ***James et al., 1996***; ***James et al., 1999***; ***Knull, 1978***; ***Lipton and Robacker, 1983***; ***Lynch and Balaban, 1987***; ***Mercer and Dunham, 1981***; ***Minakami et al., 1964***; ***Paul et al., 1979***; ***Paul, 1983***; ***Proverbio and Hoffman, 1977***; ***Weiss and Hiltbrand, 1985***; ***Whittam et al., 1964***; ***Whittam and Ager, 1965***). Our lab previously reported a link between the activity of the Na^+/K^+ pump α3-isozyme and glycolysis activation in DGCs of acute mouse hippocampal slices: the potentiation to antidromic stimulation-induced $NADH_{CYT}$ production after increasing channel-mediated influx of Na^+ with α-pompilidotoxin in the absence of external Ca^{2+} (i.e., when both Na^+ influx through the NCX and Ca^{2+} influx through channels are blocked) could be reversed by strophanthidin at low micromolar concentrations (***Díaz-García et al., 2021a***). We have shown here in DGCs that $NADH_{CYT}$ production decreases with depletion of Na^+ and increases with repletion of Na^+ (***Figure 1***), which strongly suggests that the rate of neuronal glycolysis mirrors changes in intracellular [Na^+] and in the activity of the Na^+/K^+ pump. Moreover, DGCs could not withstand complete Na^+/K^+ pump inhibition when bathed in ACSF (***Figure 3—figure supplement 1***), meaning that Na^+/K^+ pump activity is essential to counteract Na^+ leak and/or influx through Na^+-coupled transporters even when neurons are at rest.

The small NADH:NAD^+ increase produced by removing only external Ca^{2+} that we observed during our previous studies (***Díaz-García et al., 2021a***) is also consistent with a predominant influence of Na^+ on glycolysis: since Na^+ conductance through the NALCN (Na^+-leak channel, non-selective), which regulates DGC resting membrane potential and excitability (S.-Y. ***Lee et al., 2019***), is higher in the absence of external Ca^{2+} (***Kschonsak et al., 2020***; ***Lu et al., 2010***), removing external Ca^{2+} likely elevates Na^+ influx through the NALCN and increases Na^+/K^+ pump activity.

The sensitivity of glycolysis to Ca^{2+} pump activity is less clear. The small increases to the antidromic stimulation-induced ΔPeredox/ΔRCaMP ratio after applying inhibitors that target SERCA (thapsigargin; ***Figure 1—figure supplement 2***) or PMCA (E6-berbamine or calmidazolium; ***Brini et al., 2013***; ***Díaz-García et al., 2021a***) do suggest some involvement of Ca^{2+} pumps in regulating stimulation-induced Ca^{2+}_{CYT} increases, but our observations that $NADH_{CYT}$ was not increased by the elevation of Ca^{2+}_{CYT} alone, either by reverse NCX transport during ion substitution or Ca^{2+} puffs in either zero external Na^+ or 5 mM ouabain, indicate that ATP consumption associated with the direct pumping of Ca^{2+} does not have a measurable effect on glycolysis (***Figures 1–3***, and ***Figure 1—figure supplement 1***). This may indicate that Ca^{2+} pumps are either not closely coupled to glycolytic enzymes in DGCs or that Ca^{2+} pump density is small with respect to Na^+/K^+ pumps. It appears that the density of Na^+/K^+ pumps outweighs the density of Ca^{2+} pumps in hippocampus since hippocampal homogenates have ouabain-sensitive ATPase activity ~2- to 3-fold larger than Ca^{2+}-sensitive ATPase activity (***Gutierres et al., 2014***; ***Spohr et al., 2022***; ***Teixeira et al., 2020***). Even if we assume that Ca^{2+} pumps and Na^+/K^+ pumps are coupled to glycolysis equally, the lower density of Ca^{2+} pumps would make their glycolytic (and total cellular) ATP consumption less than the ATP consumed by Na^+/K^+ pumps.

Ca^{2+} pumps have an apparent $K_{0.5}$ for Ca^{2+} activation of ~0.1 μM and relatively slow maximal turnover rates of ~100 s^{-1} (characteristic of ion pumps; ***Glitsch, 2001***; ***Meyer et al., 2017***), meaning that they are well suited for tuning the resting Ca^{2+}_{CYT} but not for regulating large dynamic Ca^{2+}_{CYT} increases (***Caroni and Carafoli, 1981***). It is likely that Ca^{2+} pump transport capacity would saturate quickly in response to the 0.3–1 μM increases in Ca^{2+} during some stimulations. If an increase to Ca^{2+} pump activity was the predominant driver of $NADH_{CYT}$ production, the saturation of their Ca^{2+} transport during larger Ca^{2+}_{CYT} increases would likely cause a 'rounding off' of the Peredox LT change for stimulations where RCaMP LT changes are >0.5 ns; but the near linearity of the ΔPeredox-ΔRCaMP relationship for RCaMP LT changes of 0.05–1 ns (***Díaz-García et al., 2017***) argues against such a scenario.

The Ca^{2+}_{CYT}-dependence of aerobic glycolysis activation arises from ion transport coupling between the Na^+/Ca^{2+}-exchanger and the Na^+/K^+ pump

Our observations here that glycolysis activation in DGCs is strongly coupled to the activity of the Na^+/K^+ pump but not Ca^{2+} pumps was seemingly at odds with the ~70% reduction to antidromic stimulation-induced $NADH_{CYT}$ production by blocking Ca^{2+}_{CYT} elevation (***Díaz-García et al., 2021a***). However, the reduction to $NADH_{CYT}$ production is fully explained by the involvement of forward NCX transport in DGC Ca^{2+}_{CYT} regulation (***Figure 1F***; ***Lee et al., 2012***) and by the close coupling between the ion transport of the NCX and the Na^+/K^+ pump.

The NCX has an apparent $K_{0.5}$ for internal Ca^{2+} of ~1 μM (***Blaustein and Santiago, 1977***; ***Collins et al., 1992***; ***Miura and Kimura, 1989***) and a transport rate 10–30 times faster than the slow turnover rates of ATPases (***Blaustein and Lederer, 1999***; ***Caroni et al., 1980***). This means that NCX transport activity would be near the lower end of its total capacity when neurons are at rest (when Ca^{2+}_{CYT} is ~100 nM) but could rapidly respond to stimulation-induced Ca^{2+}_{CYT} increases and exchange it for Na^+. Unfortunately, most NCX inhibitors are unspecific or do not block the forward transport mode (***Iwamoto et al., 2004***; ***Iwamoto and Kita, 2006***; ***Secondo et al., 2015***; ***Sharikabad et al., 1997***), so the most effective way to test the involvement of forward NCX transport in glycolysis activation is to replace external Na^+ with an inert ion that cannot be transported by the NCX (i.e., choline).

The transient $NADH_{CYT}$ production evoked by Ca^{2+} puffs in 40 mM Na^+ and 0 Ca^{2+} was eliminated when external Na^+ was completely removed (i.e., replaced with choline) or when ouabain was added (***Figure 3***), meaning that both forward NCX transport and Na^+/K^+ pump activity are required for a Ca^{2+}_{CYT} elevation to measurably activate glycolysis. This unequivocally demonstrates that the exchange of Ca^{2+}_{CYT} for Na^+ by the NCX is closely coupled to Na^+ extrusion by the Na^+/K^+ pump, and that this coupling is tightly associated with the activation of glycolysis. Coupling between the NCX and Na^+/K^+ pump within discrete microdomains has also been reported in cardiac tissue (***Mohler et al., 2005***; ***Zhang et al., 2009***; ***Zhang et al., 2011***).

Strong coupling between the NCX, the Na^+/K^+ pump, and glycolysis activation can also explain two of our other observations: First, it can explain why the stimulation-induced ΔPeredox/ΔRCaMP ratio is increased by inhibition of SERCA or PMCA. Blocking either of these Ca^{2+} pumps likely increases the Ca^{2+} that is exported by the NCX, which would amplify the associated Na^+ influx through the NCX and accelerate the ATP consumption by the Na^+/K^+ pump to extrude Na^+. Second, it can explain why $NADH_{CYT}$ production was decreased when Ca^{2+}_{CYT} was elevated by reverse NCX transport (***Figure 1*** and ***Figure 1—figure supplement 1***). For reverse NCX transport to import 1 Ca^{2+} from the extracellular environment, the NCX must export 3 Na^+ (***Figure 1A***). This means that an increase to Ca^{2+}_{CYT} would occur at the same time as a decrease to intracellular $[Na^+]$, which would decrease the activity of the Na^+/K^+ pump and, consequently, decrease the rate of glycolysis and its associated $NADH_{CYT}$ production. The decrease to cytosolic NADH:NAD^+ from reverse NCX transport further supports the strong association between the energy consumed to extrude Na^+ and glycolysis and implies that even decreasing the Na^+/K^+ pump activity from an already reduced steady-state level of activity (due to the depletion of intracellular $[Na^+]$ from prior application of the 0 Na 0 Ca solution) is more influential on the rate of glycolysis than any putative strong activation of Ca^{2+} pumps by a Ca^{2+}_{CYT} increase.

The ΔPeredox/ΔRCaMP ratio evoked by Ca^{2+} puffs in 40 mM Na^+ and 0 Ca^{2+} (~0.1, ***Figure 3E***) is ~40–50% of the ΔPeredox/ΔRCaMP ratio evoked by electrical stimulation in ACSF (~0.2–0.25) (***Díaz-García et al., 2017***; ***Díaz-García et al., 2021a***), meaning that the peak activation of glycolysis relative to the Ca^{2+}_{CYT} change is smaller when evoked by Ca^{2+} puffs compared to electrical stimulation. This could be due to the absence of channel-mediated Na^+ entry during Ca^{2+} puffs compared to electrical stimulation or to the reduced external $[Na^+]$ in Ca^{2+} puff experiments (40 mM) compared to the external $[Na^+]$ during electrical stimulation in ACSF (147 mM), which would slow down the kinetics of Ca^{2+}_{CYT}-dependent Na^+ influx through forward NCX transport, consequently leading to a less potent activation of the Na^+/K^+ pump; both the quantity and the rate of Na^+ influx are likely to be important determinants of the $NADH_{CYT}$ transient amplitude and time course.

Glycolysis does not appear to be influenced by intracellular $[Na^+]$ per se, but rather by the downstream effect of $[Na^+]$ on Na^+/K^+ pump activity. If glycolytic enzymes could be directly stimulated by an increase to $[Na^+]$, then complete inhibition of the Na^+/K^+ pump should have facilitated stronger $NADH_{CYT}$ responses. But this was not the case, as $NADH_{CYT}$ responses evoked by Ca^{2+} puffs were

strongly attenuated in the presence of 5 mM ouabain (***Figure 3***), a condition that allows for Na^+ influx through the NCX but prevents Na^+ extrusion through the Na^+/K^+ pump. In contrast to the strong attenuation by 5 mM ouabain, the increase to the $NADH_{CYT}$ transients evoked by synaptic electrical stimulation after applying 5 µM ouabain in ACSF (***Figure 3—figure supplement 2***) is not as straightforward and cannot be attributed solely to an inhibition of the Na^+/K^+ pump. First, 5 µM ouabain does not substantially inhibit rodent α1-pumps (***Marks and Seeds, 1978***; ***Sweadner, 1979***); we know that 5 µM ouabain only causes partial Na^+/K^+ pump inhibition in our acute slice preparation from the mouse because it does not cause Ca^{2+}_{CYT} overload (unlike 5 mM ouabain in ACSF), which means that the plasma membrane Na^+ gradient in the presence of 5 µM ouabain remains sufficient to prevent a reversal of NCX transport. Second, the stimulation-induced Ca^{2+}_{CYT} transients were increased, which is, perhaps, reflective of an effect on synaptic release.

We think that the absence of strong $NADH_{CYT}$ responses to Ca^{2+}_{CYT} increases when Na^+ is unavailable for exchange via NCX (***Figure 1*** and ***Figure 3***) is quite informative on how both ions influence glycolysis activation, even though it is true that the rapid ionic changes that occur through channels during neuronal activity following electrical stimulation might obey somewhat different rules than the slower ionic changes we are able to make by driving ion fluxes through a secondary ion transporter. Since we have determined that $NADH_{CYT}$ production is strongly increased by an influx of Na^+ but not increased by large increases in Ca^{2+}_{CYT} (***Figures 1–3***) it is logical to infer that a transient increase to $NADH_{CYT}$ production following electrical stimulation is primarily coupled to the energy consumed to directly pump Na^+ rather than to directly pump Ca^{2+}. The amplitudes of RCaMP LT increases that we achieve with both the ion substitution experiments (***Figure 1***) and the Ca^{2+} puff experiments (***Figure 3***) are also similar to the typical amplitude of RCaMP LT increase when evoked by electrical stimulation (***Figure 4*** and ***Díaz-García et al., 2017***; ***Díaz-García et al., 2021a***), meaning that Ca^{2+}_{CYT} is increased to similar levels by all experimental paradigms regardless of their site of entry (i.e., channels or NCX).

Na^+ entry via the Na^+/Ca^{2+}-exchanger contributes substantially to total Na^+ entry in the soma

It seemed that stimulation-induced Na^+ influx via the NCX could be substantial given that a transient Ca^{2+}_{CYT} increase could only activate glycolysis if both forward NCX transport and the Na^+/K^+ pump were active (***Figure 3***) and that blocking Ca^{2+}_{CYT} strongly reduces the $NADH_{CYT}$ response (***Díaz-García et al., 2021a***). The ~50% reduction to the stimulation-induced SBFI ΔF/F peak amplitudes after blocking Ca^{2+} entry confirmed that Na^+ influx via forward NCX transport contributes greatly to the total Na^+ influx in the soma (***Figure 4***). We think it is unlikely that the reduction to the $[Na^+]$ transient after blocking Ca^{2+} entry resulted from less Na^+ entering through voltage-gated Ca^{2+} channels, since Na^+ permeation through these channels is blocked by external Ca^{2+} with a K_d of ~1 µM (***Almers and McCleskey, 1984***; ***Tsien et al., 1987***).

It is interesting to note that the positive relationship between the amplitudes of stimulation-induced transient increases to $NADH_{CYT}$ and Ca^{2+}_{CYT} appears to intercept the origin (cf. ***Figure 2***; ***Díaz-García et al., 2017***) while the relationship between the amplitudes of transient intracellular $[Na^+]$ and Ca^{2+}_{CYT} increases does not (***Figure 4—figure supplement 1***). Perhaps weaker stimulations that evoke small increases to intracellular $[Na^+]$ without a measurable increase to Ca^{2+}_{CYT} have only very weak effects on glycolysis: it could be that smaller $[Na^+]$ increases have proportionally more clearance by diffusion through the cytoplasm (***Hodgkin and Keynes, 1956***; ***Pusch and Neher, 1988***) or that the energy needed to regulate smaller $[Na^+]$ increases (without sustained Na^+ influx through forward NCX transport) is mostly derived from ATP buffering systems known to compartmentalize near sites of high ATP turnover (***Kültz and Somero, 1995***; ***Lange et al., 2002***; ***Ovádi and Saks, 2004***; ***Wallimann et al., 1992***), which could subsequently replenish their energy storage pools without large steady-state changes to glycolytic flux. Directly evaluating the role of these ATP buffering enzymes, that is, creatine kinase and adenylate kinase, in shaping the stimulation-induced transient glycolysis activation in neurons will be a key area for future exploration.

Estimation of neuronal stimulation-induced changes to intracellular $[Na^+]$ and Na^+/K^+ pump activity

SBFI calibration curves in rodent hippocampal neurons (***Baeza-Lehnert et al., 2019***; ***Diarra et al., 2001***; ***Gerkau et al., 2019***; ***Meier et al., 2006***; ***Rose et al., 1999***) reported apparent Na^+ K_d values

of 18–42 mM Na^+. However, most were performed with ouabain concentrations of only 50–100 μM, well below the millimolar concentrations needed to fully inhibit the rodent Na^+/K^+ pump α1 isozyme under physiological conditions; the relatively high ouabain-resistance of rodent α1 pumps would also be strongly increased in calibration solutions that substitute external Na^+ with high concentrations of K^+ since external K^+ competes with binding of the inhibitor to the pump's externally accessible E2 conformation (***Hansen and Skou, 1973***; ***Kanai et al., 2021***).

Despite the limitations of these in situ SBFI calibrations in rodent neurons, we use Rose et al.'s calibration of SBFI ΔF/F excited at 790 nm in brain slices with a Na^+ K_d of 26 mM (***Rose et al., 1999***) to *estimate* the stimulation-induced [Na^+] changes in our experiments (which reflect the net movement of Na^+ through influx and extrusion pathways). Our estimations assume a baseline intracellular [Na^+] of 13 mM, which is the reported value for hippocampal slice CA1 neurons (***Mondragão et al., 2016***) and nearly identical to the $K_{0.5}$ for activation of internal Na^+-dependent, ATP-induced current produced by α1β1 Na^+/K^+ pumps (which likely set baseline neuronal internal [Na^+]; ***Azarias et al., 2013***; ***Blanco, 2005***; ***Blanco and Mercer, 1998***) in excised patches when internal Na^+ is substituted with K^+ (***Meyer et al., 2017***; ***Meyer et al., 2019***; ***Meyer et al., 2020***).

The mean peak amplitude of antidromic stimulation-induced SBFI ΔF/F transients evoked in ACSF was –25.6±4.6% (***Figure 4***), reflecting an average transient [Na^+] increase of ~25 mM from baseline. How would this intracellular [Na^+] change affect neuronal Na^+/K^+ pump activity? Neurons express the α1 and α3 isoforms of the Na^+/K^+ pump (***Blanco and Mercer, 1998***). Under physiological conditions, both α1 and α3 pumps are rate limited by the binding of internal Na^+ since their $K_{0.5,Na}{}^+$ is similar to, or above, physiological intracellular [Na^+] while their $K_{0.5,K}{}^+$ is below physiological extracellular [K^+]. Activation of Na^+/K^+ pumps by internal Na^+ is also highly cooperative (Hill coefficient of ~3, corresponding to three transported Na^+ ***Crambert et al., 2000***; ***Hasler et al., 1998***; ***Meyer et al., 2017***; ***Meyer et al., 2019***; ***Meyer et al., 2020***). Based on the reported curves of Na^+/K^+ pump activation by internal Na^+ (***Crambert et al., 2000***; ***Meyer et al., 2019***), a 25 mM increase to neuronal [Na^+] from a baseline of 13 mM would likely increase peak α1β1 activity ~2-fold (to ~95% of total activity) and α3 activity ~9-fold (to ~60% of total activity).

Blocking Ca^{2+} entry reduced the antidromic stimulation-induced peak SBFI ΔF/F to –11.5±5.5% (***Figure 4***), a ~55% decrease from the transient in ACSF that corresponds nonlinearly to a reduction of the average [Na^+] increase from ~25 to ~8 mM. The estimated 8 mM stimulation-induced increase to internal [Na^+] when Ca^{2+} entry is inhibited (i.e., when Na^+ influx via forward NCX transport is reduced) would increase α1β1 activity ~1.5-fold (to ~80% of total activity) and α3 activity ~3-fold (to ~25% of total activity).

It must be noted that the proportional influence of NCX-mediated Na^+ entry on glycolysis activation could be dependent on the stimulation paradigm. Antidromic stimulation in the presence of synaptic blockers does not involve entry of Na^+ through NMDA or AMPA receptors. This means that most channel-mediated Na^+ influx that occurs from this stimulation method is through voltage-gated channels, which, in DGCs, are highly localized to the axon initial segment with weak, if any, staining in the soma (***Kole et al., 2008***; ***Kress et al., 2008***; ***Kress et al., 2010***). Thus, it is not unexpected that Na^+ influx via forward NCX transport has such a prominent effect on the antidromic stimulation-induced glycolysis activation in the soma. Soma SBFI transients evoked by either antidromic or synaptic stimulation could reach similar peak amplitudes (***Figure 4—figure supplement 1***), but the contribution of Na^+ influx through forward NCX transport to synaptically evoked [Na^+] changes could not be tested because blocking voltage-gated Ca^{2+} entry would prevent synaptic vesicle release.

NCX involvement in glycolysis activation could also vary in different neuronal compartments. Reported SBFI transient measurements indicate that antidromic stimulation-induced [Na^+] changes in the soma are typically smaller than transients in the dendrites (***Fleidervish et al., 2010***; ***Kole et al., 2008***). Measuring the ion and metabolite dynamics in dendrites will be an important step for understanding whether the mechanism of glycolysis activation in dendrites is similar to or different than the mechanism in somas.

On the mechanism of neuronal stimulation-induced aerobic glycolysis activation in somas

Based on our observations here and previously (***Díaz-García et al., 2017***; ***Díaz-García et al., 2021a***) regarding neuronal stimulation-induced [Na^+], $Ca^{2+}{}_{CYT}$, and $NADH_{CYT}$ dynamics in the soma, we can

begin to compile a more comprehensive understanding of the mechanism underlying transient aerobic glycolysis activation in response to neuronal excitation.

Neuronal stimulation immediately increases both intracellular [Na^+] and Ca^{2+}_{CYT}. The transient Ca^{2+}_{CYT} elevation lasts at most a few seconds (slightly longer than the duration of the stimulus; RCaMP1h has a $t_{1/2}$ decay of 410 ms; ***Akerboom et al., 2013***) before returning to baseline due to buffering by cytosolic proteins and removal from the cytosol. This means that any transient activation of Ca^{2+} pumps by Ca^{2+}_{CYT} would likely only be a few seconds in duration before returning to steady state. In any case, we know that this produces no measurable activation of glycolysis since similar Ca^{2+}_{CYT} transients evoked by Ca^{2+} puffs in the absence of external Na^+ or presence of ouabain were not associated with $NADH_{CYT}$ increases. It is also clear that Ca^{2+}_{CYT} is rapidly exported across the plasma membrane by forward NCX transport, which loads the neuron with Na^+. Na^+ is not buffered in the cytoplasm and is actively extruded back across the plasma membrane exclusively by the Na^+/K^+ pump. The transient intracellular [Na^+] increase lasts for a minute or more (longer than the Ca^{2+}_{CYT} transient), during which an increase to the activity of Na^+/K^+ pumps would be sustained. Both the sensitivity of $NADH_{CYT}$ production to Na^+ and the ablation of Ca^{2+}_{CYT}-evoked $NADH_{CYT}$ transients by inhibition of either forward NCX transport or the Na^+/K^+ pump demonstrate that pumping Na^+ is the predominant activity that drives the transient activation of aerobic glycolysis.

Stimulation also triggers a rapid increase to Ca^{2+}_{MITO} via MCU that can last several minutes (***Díaz-García et al., 2021a***) and requires Na^+ in order to return to the baseline (***Figure 1—figure supplement 3***). The requirement of Na^+ for Ca^{2+}_{MITO} extrusion likely indicates a Na^+-coupled Ca^{2+} efflux mechanism, as reported in other cell types (***Palty and Sekler, 2012***; ***Parpura et al., 2016***; ***Saotome et al., 2005***). Interestingly, the attenuation of Ca^{2+}_{MITO} elevation from MCU knockdown reduces the stimulation-induced cytosolic ΔPeredox/ΔRCaMP by ~50% (***Díaz-García et al., 2021a***), which is consistent with Ca^{2+}_{MITO} extrusion stimulating glycolysis. The extent to which the energetic burden of Ca^{2+}_{MITO} extrusion is placed onto glycolysis, and, more specifically, the Na^+/K^+ pump, or elsewhere will be an important area for future exploration.

Given the close coupling of the Na^+/K^+ pump to neuronal glycolysis, it will be exciting to measure how changes in Na^+/K^+ pump activity affect the flux of other glycolytic metabolites using biosensors that report lactate (***Koveal et al., 2022***; ***San Martín et al., 2013***), pyruvate (***San Martín et al., 2014***), and glucose (***Díaz-García et al., 2019***), or how changes in Na^+/K^+ pump activity affect cellular energy status (i.e., [ATP] [***Imamura et al., 2009***] and ATP:ADP [***Tantama et al., 2013***]). These investigations will ultimately provide a more complete picture of the relationship between ion homeostasis and metabolism.

Materials and methods

Key resources table

Reagent type (species) or resource	Designation	Source or reference	Identifiers	Additional information
Strain, strain background (*Mus musculus*, M and F)	C57BL/6NCrl	Charles River	RRID:IMSR_CRL:27	
Recombinant DNA reagent	AAV.CAG.Peredox.WPRE.SV40	***Mongeon et al., 2016***		Addgene #73807
Recombinant DNA reagent	AAV.hSyn.RCaMP1h.WPRE.SV40	***Akerboom et al., 2013***		
Recombinant DNA reagent	AAV.hSyn.mito-RCaMP1h.WPRE.SV40	***Díaz-García et al., 2021a***		
Chemical compound, drug	Isradipine	Abcam	Cat: ab120142, CAS: 75695-93-1	
Chemical compound, drug	NBQX (6-Nitro-7- sulfamoylbenzo [f]quinoxaline-2,3-dione, Disodium Salt)	Toronto Research Chemicals	Cat: N550005, CAS: 479347-86-9	
Chemical compound, drug	D-AP5 (D-(-)–2-Amino-5-phosphonopentanoic acid)	Abcam	Cat: ab120003, CAS: 79055-68-8	
Chemical compound, drug	Picrotoxin	Sigma-Aldrich	Cat: P1675 CAS: 124-87-8	

Continued on next page

Continued

Reagent type (species) or resource	Designation	Source or reference	Identifiers	Additional information
Chemical compound, drug	$CdCl_2$	Sigma-Aldrich	Cat: 202908, CAS: 10108-64-2	
Chemical compound, drug	Poly-L-lysine	Sigma-Aldrich	Cat: P4832	
Chemical compound, drug	Aminooxyacetate (O-(carboxymethyl) hydroxylamine hemihydrate)	Sigma-Aldrich	Cat: C13408 CAS: 2921-14-4	
Chemical compound, drug	Pyruvic acid	Sigma-Aldrich	Cat: 107360, CAS: 127-17-3	
Chemical compound, drug	Thapsigargin	Santa Cruz Biotechnology	Cat: sc-24017A, CAS: 67526-95-8	
Chemical compound, drug	Ouabain	Sigma-Aldrich	Cat: O3125, CAS: 11018-89-6	
Chemical compound, drug	SBFI K^+ salt (fluorescent dye)	Ion Biosciences	Cat: 2022B	
Other	Glass capillaries, Borosilicate, standard wall, no filament, 4 in., O.D. 1.5 mm	WPI	Cat: 1B150-4	For microelectrodes and pipettes
Other	Glass coverslips, 12 mm circle No.1	VWR	Cat: 48366–251	For brain slice handling

Animals

Experiments were performed using male and female wild-type mice (C57BL/6NCrl, Charles River Laboratories), which were housed in a barrier facility in individually ventilated cages with ad libitum access to standard chow (PicoLab 5053). All experiments followed approved IACUC protocols and the NIH Guide for the Care and Use of Laboratory Animals and Animal Welfare Act. All procedures were approved by the Harvard Medical Area Standing Committee on Animals.

Viral vectors

DNA constructs encoding Peredox, RCaMP, or mito-RCaMP biosensors were packaged into adeno-associated virus (AAV) vectors using either the Penn Vector Core at University of Pennsylvania or the Viral Core Facility at Children's Hospital in Boston, MA. AAV vectors encoding RCaMP were also produced in our laboratory, as previously described (***Kimura et al., 2019***). The AAV8 serotype was used for Peredox and AAV9 for RCaMP and mito-RCaMP. AAVs were aliquoted and stored at –80°C.

Intracranial injections

Postnatal day 1 or 2, mice were injected intracranially with AAV to express biosensors in the hippocampus (***Díaz-García et al., 2021b***). Mice were cryoanesthetized and injected with 150 nL AAV using an UltraMicroPump III (WPI, Sarasota, FL) microinjector in two locations of each hemisphere at the following coordinates relative to lambda: (1) 0 mm anterior-posterior; ±1.9 mm medial-lateral; –2.0 mm dorsal-ventral; and (2) 0 mm anterior-posterior; ±2.0 mm medial-lateral; –2.3 mm dorsal-ventral. Injected pups were placed on a heating pad and allowed to recover before being returned to their cages and were administered daily ketoprofen (10 mg/kg) subcutaneously for up to 3 days.

Hippocampal slice preparation

Injected mice between 14 and 24 days old were anesthetized with isoflurane, decapitated, and the brain was removed into ice-cold slicing solution containing (in mM) 87 NaCl, 2.5 KCl, 1.25 NaH_2PO_4, 25 $NaHCO_3$, 75 sucrose, 25 D-glucose, 0.5 $CaCl_2$, and 7 $MgCl_2$ (~335 mOsm/kg) and bubbled with 95% O_2 and 5% CO_2. The brain was glued by the dorsal side, embedded into 2% agarose in phosphate-buffered saline, and submerged in a chamber with ice-cold slicing solution. Horizontal 275 µm brain slices were cut using a compresstome (VF-310-0Z, Precisionary) and immediately transferred to a chamber with ACSF containing (in mM) 120 NaCl, 2.5 KCl, 1 NaH_2PO_4, 26 $NaHCO_3$, 10 D-glucose, 2 $CaCl_2$, and 1 $MgCl_2$ (~290 mOsm/kg) that was warmed to 36°C and bubbled with 95% O_2 and 5% CO_2. The slices rested on a mesh bottom to adequately perfuse both sides of the tissue. After 35 min, the chamber was cooled to room temperature and the brain slices therein were used for the next 4 hr.

Recording solutions and pharmacology

The brain slices were adhered to glass coverslips coated with poly-L-lysine (P4832, Sigma-Aldrich), placed in a bath chamber mounted to the microscope, and superfused with solutions maintained at 33–34°C and bubbled with 95% O_2 and 5% CO_2 at a rate of 5 mL/min. All solutions were ~290 mOsm/kg and contained 25 µM D-AP5, 5 µM NBQX, and 100 µM picrotoxin (unless otherwise specified) to block synaptic transmission. Ca^{2+}-free solution contained (in mM) 120 NaCl, 2.5 KCl, 1 NaH_2PO_4, 26 $NaHCO_3$, 10 D-glucose, and 4.1 $MgCl_2$. Na^+- and Ca^{2+}-free solution contained (in mM) 120 Choline-Cl, 1.5 KCl, 1 KH_2PO_4, 26 Choline-HCO_3, 10 D-glucose, and 4.1 $MgCl_2$. 1 mM EGTA was added to the Ca^{2+}-free solutions from a 0.5 M stock.

For Ca^{2+}-puff experiments, the 40 mM Na^+ and Ca^{2+}-free solution was obtained by mixing Ca^{2+}-free solution with Na^+- and Ca^{2+}-free solution; all solutions for those experiments also contained 0.1 mM EGTA.

Thapsigargin (1 µM) was added from a 10 mM stock in DMSO. Aminooxyacetate (AOA, 10 mM) was added from a 2 M stock in water. Pyruvate (1.5 mM) was added from a 1 M aqueous stock, pH 7.3 with *N*-methyl-D-glucamine. Ouabain was either directly dissolved (for 2–5 mM) prior to recording or added from a 5 mM stock in water (for 5 µM). Isradipine (3 µM) was added from a 50 mM DMSO stock. $CdCl_2$ (20 µM) was added from a 100 mM stock in water.

Electrical stimulation

Stimulation trains (of 100 µs pulse width) were delivered as previously described (***Díaz-García et al., 2017***; ***Díaz-García et al., 2021a***) using a concentric bipolar electrode (FHC, Bowdoin, ME) mounted on a motorized micromanipulator (Burleigh PCS-6000, ThorLabs, Sterling, VA) and connected to an A360 stimulus isolation unit (WPI, Sarasota, FL). DGCs were stimulated antidromically (100 pulses, 50 Hz, 750–1500 µA) by placing the electrode in the hippocampal hilus, or synaptically (60 pulses, 20 Hz, 100–500 µA) by placing the electrode in the molecular layer.

Ca^{2+} puffs

Borosilicate glass pipettes (with a tip diameter of 5 µm and resistance of 1 MΩ when filled with ACSF) were fabricated on a micropipette puller (P-97 Flaming/Brown, Sutter Instruments), backfilled with 100–250 mM $CaCl_2$ and placed into a pipette holder mounted on a motorized micromanipulator with a closed pressure system connected to a 1 mL syringe. The pipette tip was placed adjacent to groups of DGCs expressing Peredox and RCaMP biosensors. Pressure delivery was controlled by a solenoid valve (NResearch) in series with the syringe line that was triggered by a digital/analog actuator (NTE Electronics). Positive pressure was applied using the syringe, and Ca^{2+} puffs were delivered by opening the solenoid for 0.5–5 s beginning 300 ms after the start of image acquisition.

Single-cell electroporation of SBFI

Sodium-binding benzofuran isophthalate (SBFI) is a fluorescent Na^+-indicator (***Harootunian et al., 1989***). We loaded the SBFI K^+ salt (Ion Biosciences, San Marcos, TX) version into DGCs using single-cell electroporation methods derived from ***Nevian and Helmchen, 2007***; we chose this method rather than loading by patch pipette to avoid diluting cytoplasmic metabolites and soluble expressed biosensor, and also to avoid potentially toxic effects on the slice from applying Pluronic-F127 and DMSO to load the membrane-permeant SBFI-acetoxymethyl ester version.

Borosilicate glass pipettes were fabricated (with a tip diameter of 1 µm and resistance of 3 MΩ when filled with ACSF), loaded with 4 mM SBFI-K^+ in distilled H_2O, and placed onto a pipette holder with a closed pressure system mounted on a motorized micromanipulator. The SBFI solution was contacted by a chlorided silver wire connected to an A360 stimulus isolation unit, and an Ag-AgCl reference electrode was placed in the bath chamber and connected to the same stimulation device. The pipette tip was placed directly next to the soma of an RCaMP-expressing DGC. No positive pressure was applied. A single 10 ms pulse of negative 1.0–1.2 µA loaded the DGC with SBFI. Recovery of the membrane potential from these electroporation pulses takes ~1–2 min (***Nevian and Helmchen, 2007***). We waited ≥15 min after the electroporation to start the image acquisition and electrically stimulate the SBFI-loaded, RCaMP-expressing DGCs.

The intracellular [dye] from electroporation is estimated to be ~20% of the pipette concentration (***Nevian and Helmchen, 2007***). Thus, the intracellular [Na^+] will not be substantially buffered by

the ~0.5–1 mM [SBFI] in our recordings (***Fleidervish et al., 2010***; ***Mondragão et al., 2016***), meaning that intracellular [Na^+] is set by cellular mechanisms and SBFI merely responds to changes in [Na^+]. Also, the complexation of Na^+ with crown ether molecules (the Na^+-sensitive moiety of SBFI) is nearly diffusion-controlled, with very rapid rates of formation and dissociation (***Adamic et al., 1986***; ***Liesegang et al., 1977***). This means that the response time of SBFI fluorescence changes should be fast compared to almost all neuronal processes.

Two-photon fluorescence imaging

Fluorescence imaging data were acquired using a Thorlabs Bergamo II microscope (Thorlabs Imaging Systems, Sterling, VA) equipped with an Olympus LUMPLFLN 60×/W (NA 1.0) objective lens, hybrid photodetectors R11322U-40 (Hamamatsu Photonics, Shizuoka, Japan), and a Chameleon Vision-S tunable Ti-Sapphire mode-locked laser (80 MHz,~75 fs pulses; Coherent, Santa Clara, CA). The excitation wavelength was 790 nm. Fluorescence emission light from the Peredox and RCaMP biosensors was split with an FF562-Di03 dichroic mirror and bandpass filtered for green (FF01-525/50) and red (FF01-641/75) light; a red 670/50 bandpass filter was used for experiments where SBFI and RCaMP were multiplexed. The photodetector and laser sync signals were preamplified and then digitized at 1.25 GHz using a field-programmable gate array board (PC720 with FMC125 and FMC122 modules, 4DSP, Austin, TX). A modified version of the ScanImage software written in Matlab (***Pologruto et al., 2003***) (provided by B. Sabatini and modified by G.Y.) controlled the laser, microscope, and image acquisition (128×128 pixels, scanning rate of 2 ms per line).

Time-correlated single-photon counting was performed using laboratory-built firmware and software to determine the arrival time of each photon relative to the laser pulse. The fluorescence LT was determined from a nonlinear least-squares fit to the photon arrival histograms in Matlab (Mathworks, Natick, MA) convolved with a Gaussian for the impulse response function (***Yasuda et al., 2006***). Fluorescence intensity was determined from the total photon counts.

Data analysis

Fluorescence images were analyzed offline using Matlab R2014b software. Regions of interest (ROIs) were defined around individual DGC somas and photon statistics were calculated for all pixels within the ROI. LT values were calculated by fitting the photon arrival histograms with a biexponential decay function (convolved with a Gaussian for the impulse response function [***Yasuda et al., 2006***] up to 8 ns after the peak photon arrival time). The time constant of this fit is denoted as the 'tau8' value (***Díaz-García et al., 2019***); using tau8 values minimizes both the fit variability (by restricting the averaging to the approximate time window of the actual data) and the variability between the LTs recorded on different experimental setups with different data acquisition windows.

RCaMP signals were unmixed from Peredox as previously described (***Díaz-García et al., 2017***; ***Díaz-García et al., 2021a***). RCaMP signals were unmixed from SBFI bleedthrough into the red 670/50 bandpass filter following previous methods (***Díaz-García et al., 2017***) but using an unmixing ratio of 0.053, since the red channel photon counts from SBFI-loaded DGCs (not expressing RCaMP) were (mean ± SD) 5.3±1.2% (n=42) of the green channel photon counts. Stimulation-induced SBFI intensity recordings were analyzed using Origin 8.1 (OriginLab, Northampton, MA) and Python 3 (https://www.anaconda.com/, RRID – SRC:008394, Numpy and Pandas libraries). Individual transient fluorescence intensity traces were baseline subtracted and the peak ΔF/F was determined as the minimum intensity value.

Average time traces of transient fluorescence LT or intensity changes were created using Python. Data acquisition times for individual fluorescence traces were binned to the nearest second for data acquired before and after the stimulation event (which were acquired every 10–60 s) or the nearest 10 ms for data acquired during the stimulation (which were acquired every ~250 ms). Traces from all stimulation-induced transients in the data set were interpolated and merged onto a single time axis, from which the means, standard deviations, and standard error of the means were determined.

Statistical analysis was performed using Origin 8.1 software. Data sets were tested for normality (α=0.05) using a Shapiro-Wilk test. Data sets that met normality criteria were compared using a paired t-test, or two-sample t-test. Data sets that did not meet normality criteria were compared using a paired sample Wilcoxon test or Mann-Whitney test for unpaired samples. Data are reported as mean

± standard deviation (unless otherwise indicated). For box plots, the means are indicated by the filled square, medians are indicated by the horizontal bar, and 5–95% ranges are indicated by whiskers.

Figures were created using Origin 8.1 and PowerPoint (Microsoft, Redmond, WA).

Reagents

All chemical reagents used to make the brain slicing and artificial cerebrospinal fluid (ACSF) solutions were obtained from Sigma-Aldrich (St. Louis, MO).

Acknowledgements

The authors thank the members of the Yellen lab for their valuable discussions. The authors thank Dr Juan Ramón Martínez François and Dr Pablo Artigas for their critical review of the manuscript. This work was supported by research grants from the National Institutes of Health (R01 NS102586 and R01 GM124038 to GY) and Postdoctoral Fellowships from the National Institutes of Health (F32 NS116105 to DJM and F32 NS100331 to CMDG) and the Harvard Mahoney Neuroscience Institute Fund (to DJM).

Additional information

Competing interests

Gary Yellen: Reviewing editor, *eLife*. The other authors declare that no competing interests exist.

Funding

Funder	Grant reference number	Author
National Institute of Neurological Disorders and Stroke	R01 NS102586	Gary Yellen
National Institute of General Medical Sciences	R01 GM124038	Gary Yellen
National Institute of Neurological Disorders and Stroke	F32 NS116105	Dylan J Meyer
National Institute of Neurological Disorders and Stroke	F32 NS100331	Carlos Manlio Díaz-García
Harvard Mahoney Neuroscience Institute	Postdoctoral Fellowship	Dylan J Meyer

The funders had no role in study design, data collection and interpretation, or the decision to submit the work for publication.

Author contributions

Dylan J Meyer, Conceptualization, Software, Funding acquisition, Investigation, Methodology, Writing - original draft, Writing – review and editing; Carlos Manlio Díaz-García, Conceptualization, Funding acquisition, Investigation, Methodology, Writing – review and editing; Nidhi Nathwani, Mahia Rahman, Investigation, Methodology, Writing – review and editing; Gary Yellen, Conceptualization, Supervision, Funding acquisition, Methodology, Writing – review and editing

Author ORCIDs

Dylan J Meyer http://orcid.org/0000-0001-8453-3813
Carlos Manlio Díaz-García http://orcid.org/0000-0002-4352-2496
Gary Yellen http://orcid.org/0000-0003-4228-7866

Ethics

All experiments were performed in compliance with the NIH Guide for the Care and Use of Laboratory Animals and the Animal Welfare Act. The Harvard Medical Area Standing Committee on Animals

approved all procedures involving animals. (Animal Welfare Assurance Number A3431-01, Protocol IS00001113-3).

Decision letter and Author response

Decision letter https://doi.org/10.7554/eLife.81645.sa1
Author response https://doi.org/10.7554/eLife.81645.sa2

Additional files

Supplementary files

- MDAR checklist

Data availability

All data generated or analysed during this study are included in the manuscript.

References

Adamic RJ, Lloyd BA, Eyring EM, Petrucci S, Bartsch RA, Pugia MJ, Knudsen BE, Liu Y, Desai DH. 1986. Sodium ion complexation by ionizable crown ethers in methanol-water solvents. A thermodynamic and kinetic evaluation of sidearm interaction. *The Journal of Physical Chemistry* **90**:6571–6576. DOI: https://doi.org/10.1021/j100282a030

Akerboom J, Carreras Calderón N, Tian L, Wabnig S, Prigge M, Tolö J, Gordus A, Orger MB, Severi KE, Macklin JJ, Patel R, Pulver SR, Wardill TJ, Fischer E, Schüler C, Chen TW, Sarkisyan KS, Marvin JS, Bargmann CI, Kim DS, et al. 2013. Genetically encoded calcium indicators for multi-color neural activity imaging and combination with optogenetics. *Frontiers in Molecular Neuroscience* **6**:2. DOI: https://doi.org/10.3389/fnmol.2013.00002, PMID: 23459413

Almers W, McCleskey EW. 1984. Non-selective conductance in calcium channels of frog muscle: calcium selectivity in a single-file pore. *The Journal of Physiology* **353**:585–608. DOI: https://doi.org/10.1113/jphysiol.1984.sp015352, PMID: 6090646

Ames A. 2000. CNS energy metabolism as related to function. *Brain Research. Brain Research Reviews* **34**:42–68. DOI: https://doi.org/10.1016/s0165-0173(00)00038-2, PMID: 11086186

Andersen BJ, Marmarou A. 1992. Functional compartmentalization of energy production in neural tissue. *Brain Research* **585**:190–195. DOI: https://doi.org/10.1016/0006-8993(92)91206-t, PMID: 1511302

Astrup J, Sørensen PM, Sørensen HR. 1981. Oxygen and glucose consumption related to Na^+-K^+ transport in canine brain. *Stroke* **12**:726–730. DOI: https://doi.org/10.1161/01.str.12.6.726, PMID: 7303061

Attwell D, Laughlin SB. 2001. An energy budget for signaling in the grey matter of the brain. *Journal of Cerebral Blood Flow and Metabolism* **21**:1133–1145. DOI: https://doi.org/10.1097/00004647-200110000-00001, PMID: 11598490

Attwell D, Iadecola C. 2002. The neural basis of functional brain imaging signals. *Trends in Neurosciences* **25**:621–625. DOI: https://doi.org/10.1016/s0166-2236(02)02264-6, PMID: 12446129

Azarias G, Kruusmägi M, Connor S, Akkuratov EE, Liu XL, Lyons D, Brismar H, Broberger C, Aperia A. 2013. A specific and essential role for Na, K-ATPase α3 in neurons co-expressing α1 and α3. *The Journal of Biological Chemistry* **288**:2734–2743. DOI: https://doi.org/10.1074/jbc.M112.425785, PMID: 23195960

Baeza-Lehnert F, Saab AS, Gutiérrez R, Larenas V, Díaz E, Horn M, Vargas M, Hösli L, Stobart J, Hirrlinger J, Weber B, Barros LF. 2019. Non-canonical control of neuronal energy status by the Na^+ pump. *Cell Metabolism* **29**:668–680. DOI: https://doi.org/10.1016/j.cmet.2018.11.005, PMID: 30527744

Balaban RS, Bader JP. 1984. Studies on the relationship between glycolysis and (Na^+ + K^+) -ATPase in cultured cells. *Biochimica et Biophysica Acta* **804**:419–426. DOI: https://doi.org/10.1016/0167-4889(84)90069-7, PMID: 6087923

Berjukow S, Marksteiner R, Gapp F, Sinnegger MJ, Hering S. 2000. Molecular mechanism of calcium channel block by isradipine. *Journal of Biological Chemistry* **275**:22114–22120. DOI: https://doi.org/10.1074/jbc.M908836199, PMID: 10766758

Biondo ED, Spontarelli K, Ababioh G, Méndez L, Artigas P. 2021. Diseases caused by mutations in the Na^+/K^+ pump α1 gene *ATP1A1*. *American Journal of Physiology. Cell Physiology* **321**:C394–C408. DOI: https://doi.org/10.1152/ajpcell.00059.2021

Blanco G, Mercer RW. 1998. Isozymes of the Na-K-ATPase: heterogeneity in structure, diversity in function. *American Journal of Physiology-Renal Physiology* **275**:F633–F650. DOI: https://doi.org/10.1152/ajprenal.1998.275.5.F633

Blanco G. 2005. Na, K-ATPase subunit heterogeneity as a mechanism for tissue-specific ion regulation. *Seminars in Nephrology* **25**:292–303. DOI: https://doi.org/10.1016/j.semnephrol.2005.03.004, PMID: 16139684

Blaustein MP, Santiago EM. 1977. Effects of internal and external cations and of ATP on sodium-calcium and calcium-calcium exchange in squid axons. *Biophysical Journal* **20**:79–111. DOI: https://doi.org/10.1016/S0006-3495(77)85538-0, PMID: 901903

Blaustein MP, Lederer WJ. 1999. Sodium/calcium exchange: its physiological implications. *Physiological Reviews* **79**:763–854. DOI: https://doi.org/10.1152/physrev.1999.79.3.763, PMID: 10390518

Brini M, Calì T, Ottolini D, Carafoli E. 2013. The plasma membrane calcium pump in health and disease. *The FEBS Journal* **280**:5385–5397. DOI: https://doi.org/10.1111/febs.12193, PMID: 23413890

Calì T, Brini M, Carafoli E. 2018. The PMCA pumps in genetically determined neuronal pathologies. *Neuroscience Letters* **663**:2–11. DOI: https://doi.org/10.1016/j.neulet.2017.11.005, PMID: 29155350

Caroni P, Reinlib L, Carafoli E. 1980. Charge movements during the Na^+-Ca^{2+} exchange in heart sarcolemmal vesicles. *PNAS* **77**:6354–6358. DOI: https://doi.org/10.1073/pnas.77.11.6354, PMID: 6935649

Caroni P, Carafoli E. 1981. The Ca^{2+}-pumping ATPase of heart sarcolemma. Characterization, calmodulin dependence, and partial purification. *The Journal of Biological Chemistry* **256**:3263–3270 PMID: 6451626.

Chemaly ER, Troncone L, Lebeche D. 2018. SERCA control of cell death and survival. *Cell Calcium* **69**:46–61. DOI: https://doi.org/10.1016/j.ceca.2017.07.001, PMID: 28747251

Collins A, Somlyo AV, Hilgemann DW. 1992. The giant cardiac membrane patch method: stimulation of outward Na^+-Ca^{2+} exchange current by MgATP. *The Journal of Physiology* **454**:27–57. DOI: https://doi.org/10.1113/jphysiol.1992.sp019253, PMID: 1335502

Contreras L, Satrústegui J. 2009. Calcium signaling in brain mitochondria. *Journal of Biological Chemistry* **284**:7091–7099. DOI: https://doi.org/10.1074/jbc.M808066200

Crambert G, Hasler U, Beggah AT, Yu C, Modyanov NN, Horisberger JD, Lelièvre L, Geering K. 2000. Transport and pharmacological properties of nine different human Na, K-ATPase isozymes. *The Journal of Biological Chemistry* **275**:1976–1986. DOI: https://doi.org/10.1074/jbc.275.3.1976, PMID: 10636900

Dhar-Chowdhury P, Malester B, Rajacic P, Coetzee WA. 2007. The regulation of ion channels and transporters by glycolytically derived ATP. *Cellular and Molecular Life Sciences* **64**:3069–3083. DOI: https://doi.org/10.1007/s00018-007-7332-3

Diarra A, Sheldon C, Church J. 2001. In situ calibration and $[H^+]$ sensitivity of the fluorescent Na^+ indicator SBFI. *American Journal of Physiology. Cell Physiology* **280**:C1623–C1633. DOI: https://doi.org/10.1152/ajpcell.2001.280.6.C1623, PMID: 11350758

Díaz-García CM, Mongeon R, Lahmann C, Koveal D, Zucker H, Yellen G. 2017. Neuronal stimulation triggers neuronal glycolysis and not lactate uptake. *Cell Metabolism* **26**:361–374. DOI: https://doi.org/10.1016/j.cmet.2017.06.021, PMID: 28768175

Díaz-García CM, Lahmann C, Martínez-François JR, Li B, Koveal D, Nathwani N, Rahman M, Keller JP, Marvin JS, Looger LL, Yellen G. 2019. Quantitative in vivo imaging of neuronal glucose concentrations with a genetically encoded fluorescence lifetime sensor. *Journal of Neuroscience Research* **97**:946–960. DOI: https://doi.org/10.1002/jnr.24433, PMID: 31106909

Díaz-García CM, Meyer DJ, Nathwani N, Rahman M, Martínez-François JR, Yellen G. 2021a. The distinct roles of calcium in rapid control of neuronal glycolysis and the tricarboxylic acid cycle. *eLife* **10**:e64821. DOI: https://doi.org/10.7554/eLife.64821

Díaz-García CM, Nathwani N, Martínez-François JR, Yellen G. 2021b. Delivery of AAV for expression of fluorescent biosensors in juvenile mouse hippocampus. *Bio-Protocol* **11**:e4259. DOI: https://doi.org/10.21769/BioProtoc.4259, PMID: 35087918

Dzeja PP, Terzic A. 2003. Phosphotransfer networks and cellular energetics. *The Journal of Experimental Biology* **206**:2039–2047. DOI: https://doi.org/10.1242/jeb.00426, PMID: 12756286

Engl E, Attwell D. 2015. Non-signalling energy use in the brain. *The Journal of Physiology* **593**:3417–3429. DOI: https://doi.org/10.1113/jphysiol.2014.282517, PMID: 25639777

Fleidervish IA, Lasser-Ross N, Gutnick MJ, Ross WN. 2010. Na^+ imaging reveals little difference in action potential-evoked Na^+ influx between axon and soma. *Nature Neuroscience* **13**:852–860. DOI: https://doi.org/10.1038/nn.2574, PMID: 20543843

Fothergill-Gilmore LA, Michels PAM. 1993. Evolution of glycolysis. *Progress in Biophysics and Molecular Biology* **59**:105–235. DOI: https://doi.org/10.1016/0079-6107(93)90001-z, PMID: 8426905

Fox PT, Raichle ME. 1986. Focal physiological uncoupling of cerebral blood flow and oxidative metabolism during somatosensory stimulation in human subjects. *PNAS* **83**:1140–1144. DOI: https://doi.org/10.1073/pnas.83.4.1140, PMID: 3485282

Fox PT, Raichle ME, Mintun MA, Dence C. 1988. Nonoxidative glucose consumption during focal physiologic neural activity. *Science* **241**:462–464. DOI: https://doi.org/10.1126/science.3260686, PMID: 3260686

Gerkau NJ, Lerchundi R, Nelson JSE, Lantermann M, Meyer J, Hirrlinger J, Rose CR. 2019. Relation between activity-induced intracellular sodium transients and ATP dynamics in mouse hippocampal neurons. *The Journal of Physiology* **597**:5687–5705. DOI: https://doi.org/10.1113/JP278658, PMID: 31549401

Glitsch HG. 2001. Electrophysiology of the sodium-potassium-ATPase in cardiac cells. *Physiological Reviews* **81**:1791–1826. DOI: https://doi.org/10.1152/physrev.2001.81.4.1791, PMID: 11581502

Gutierres JM, Carvalho FB, Schetinger MRC, Marisco P, Agostinho P, Rodrigues M, Rubin MA, Schmatz R, da Silva CR, de P Cognato G, Farias JG, Signor C, Morsch VM, Mazzanti CM, Bogo M, Bonan CD, Spanevello R. 2014. Anthocyanins restore behavioral and biochemical changes caused by streptozotocin-induced sporadic dementia of Alzheimer's type. *Life Sciences* **96**:7–17. DOI: https://doi.org/10.1016/j.lfs.2013.11.014, PMID: 24291256

Hansen O, Skou JC. 1973. A study on the influence of the concentration of Mg^{2+}, P_i, K^+, Na^+, and tris on (Mg^{2+} + P_i) -supported g-strophanthin binding to (Na^+ + K^+) activated ATPase from ox brain. *Biochimica et Biophysica Acta* **311**:51–66. DOI: https://doi.org/10.1016/0005-2736(73)90254-x, PMID: 4268760

Harootunian AT, Kao JP, Eckert BK, Tsien RY. 1989. Fluorescence ratio imaging of cytosolic free Na^+ in individual fibroblasts and lymphocytes. *Journal of Biological Chemistry* **264**:19458–19467. DOI: https://doi.org/10.1016/S0021-9258(19)47322-5

Harris JJ, Jolivet R, Attwell D. 2012. Synaptic energy use and supply. *Neuron* **75**:762–777. DOI: https://doi.org/10.1016/j.neuron.2012.08.019, PMID: 22958818

Hasin Y, Barry WH. 1984. Myocardial metabolic inhibition and membrane potential, contraction, and potassium uptake. *The American Journal of Physiology* **247**:H322–H329. DOI: https://doi.org/10.1152/ajpheart.1984.247.2.H322, PMID: 6087686

Hasler U, Wang X, Crambert G, Béguin P, Jaisser F, Horisberger JD, Geering K. 1998. Role of beta-subunit domains in the assembly, stable expression, intracellular routing, and functional properties of Na, K-ATPase. *The Journal of Biological Chemistry* **273**:30826–30835. DOI: https://doi.org/10.1074/jbc.273.46.30826, PMID: 9804861

Hellstrand P, Jorup C, Lydrup ML. 1984. O_2 consumption, aerobic glycolysis and tissue phosphagen content during activation of the NA^+/K^+ pump in rat portal vein. *Pflugers Archiv* **401**:119–124. DOI: https://doi.org/10.1007/BF00583871, PMID: 6089095

Hodgkin AL, Keynes RD. 1956. Experiments on the injection of substances into squid giant axons by means of a microsyringe. *The Journal of Physiology* **131**:592–616. DOI: https://doi.org/10.1113/jphysiol.1956.sp005485, PMID: 13320357

Howarth C, Gleeson P, Attwell D. 2012. Updated energy budgets for neural computation in the neocortex and cerebellum. *Journal of Cerebral Blood Flow and Metabolism* **32**:1222–1232. DOI: https://doi.org/10.1038/jcbfm.2012.35, PMID: 22434069

Hung YP, Albeck JG, Tantama M, Yellen G. 2011. Imaging cytosolic NADH-NAD^+ redox state with a genetically encoded fluorescent biosensor. *Cell Metabolism* **14**:545–554. DOI: https://doi.org/10.1016/j.cmet.2011.08.012, PMID: 21982714

Imamura H, Nhat KPH, Togawa H, Saito K, Iino R, Kato-Yamada Y, Nagai T, Noji H. 2009. Visualization of ATP levels inside single living cells with fluorescence resonance energy transfer-based genetically encoded indicators. *PNAS* **106**:15651–15656. DOI: https://doi.org/10.1073/pnas.0904764106, PMID: 19720993

Iwamoto T, Kita S, Uehara A, Imanaga I, Matsuda T, Baba A, Katsuragi T. 2004. Molecular determinants of Na^+/$Ca2^+$ exchange (NCX1) inhibition by SEA0400. *The Journal of Biological Chemistry* **279**:7544–7553. DOI: https://doi.org/10.1074/jbc.M310491200, PMID: 14660663

Iwamoto T, Kita S. 2006. YM-244769, a novel Na^+/Ca^{2+} exchange inhibitor that preferentially inhibits NCX3, efficiently protects against hypoxia/reoxygenation-induced SH-SY5Y neuronal cell damage. *Molecular Pharmacology* **70**:2075–2083. DOI: https://doi.org/10.1124/mol.106.028464, PMID: 16973719

James JH, Fang CH, Schrantz SJ, Hasselgren PO, Paul RJ, Fischer JE. 1996. Linkage of aerobic glycolysis to sodium-potassium transport in rat skeletal muscle. Implications for increased muscle lactate production in sepsis. *The Journal of Clinical Investigation* **98**:2388–2397. DOI: https://doi.org/10.1172/JCI119052, PMID: 8941658

James JH, Wagner KR, King JK, Leffler RE, Upputuri RK, Balasubramaniam A, Friend LA, Shelly DA, Paul RJ, Fischer JE. 1999. Stimulation of both aerobic glycolysis and Na^+-K^+-ATPase activity in skeletal muscle by epinephrine or amylin. *The American Journal of Physiology* **277**:E176–E186. DOI: https://doi.org/10.1152/ajpendo.1999.277.1.E176, PMID: 10409142

Kanai R, Cornelius F, Ogawa H, Motoyama K, Vilsen B, Toyoshima C. 2021. Binding of cardiotonic steroids to Na^+,K^+-ATPase in the E2P state. *PNAS* **118**:e2020438118. DOI: https://doi.org/10.1073/pnas.2020438118

Kaplan JH. 2002. Biochemistry of Na, K-ATPase. *Annual Review of Biochemistry* **71**:511–535. DOI: https://doi.org/10.1146/annurev.biochem.71.102201.141218, PMID: 12045105

Kemp RG, Foe LG. 1983. Allosteric regulatory properties of muscle phosphofructokinase. *Molecular and Cellular Biochemistry* **57**:147–154. DOI: https://doi.org/10.1007/BF00849191, PMID: 6228716

Kimura T, Ferran B, Tsukahara Y, Shang Q, Desai S, Fedoce A, Pimentel DR, Luptak I, Adachi T, Ido Y, Matsui R, Bachschmid MM. 2019. Production of adeno-associated virus vectors for in vitro and in vivo applications. *Scientific Reports* **9**:13601. DOI: https://doi.org/10.1038/s41598-019-49624-w, PMID: 31537820

Knull HR. 1978. Association of glycolytic enzymes with particulate fractions from nerve endings. *Biochimica et Biophysica Acta* **522**:1–9. DOI: https://doi.org/10.1016/0005-2744(78)90316-9, PMID: 620035

Kole MHP, Ilschner SU, Kampa BM, Williams SR, Ruben PC, Stuart GJ. 2008. Action potential generation requires a high sodium channel density in the axon initial segment. *Nature Neuroscience* **11**:178–186. DOI: https://doi.org/10.1038/nn2040, PMID: 18204443

Koveal D, Rosen PC, Meyer DJ, Díaz-García CM, Wang Y, Cai LH, Chou PJ, Weitz DA, Yellen G. 2022. A high-throughput multiparameter screen for accelerated development and optimization of soluble genetically encoded fluorescent biosensors. *Nature Communications* **13**:2919. DOI: https://doi.org/10.1038/s41467-022-30685-x, PMID: 35614105

Kress GJ, Dowling MJ, Meeks JP, Mennerick S. 2008. High threshold, proximal initiation, and slow conduction velocity of action potentials in dentate granule neuron mossy fibers. *Journal of Neurophysiology* **100**:281–291. DOI: https://doi.org/10.1152/jn.90295.2008, PMID: 18480368

Kress GJ, Dowling MJ, Eisenman LN, Mennerick S. 2010. Axonal sodium channel distribution shapes the depolarized action potential threshold of dentate granule neurons. *Hippocampus* **20**:558–571. DOI: https://doi.org/10.1002/hipo.20667, PMID: 19603521

Kschonsak M, Chua HC, Noland CL, Weidling C, Clairfeuille T, Bahlke OØ, Ameen AO, Li ZR, Arthur CP, Ciferri C, Pless SA, Payandeh J. 2020. Structure of the human sodium leak channel NALCN. *Nature* **587**:313–318. DOI: https://doi.org/10.1038/s41586-020-2570-8, PMID: 32698188

Kültz D, Somero GN. 1995. Ion transport in gills of the euryhaline fish *Gillichthys mirabilis* is facilitated by a phosphocreatine circuit. *The American Journal of Physiology* **268**:R1003–R1012. DOI: https://doi.org/10.1152/ajpregu.1995.268.4.R1003, PMID: 7733382

Lakowicz JR. 2006. Principles of Fluorescence Spectroscopy. 3rd ed. Springer. DOI: https://doi.org/10.1007/978-0-387-46312-4

Lange S, Auerbach D, McLoughlin P, Perriard E, Schäfer BW, Perriard JC, Ehler E. 2002. Subcellular targeting of metabolic enzymes to titin in heart muscle may be mediated by DRAL/FHL-2. *Journal of Cell Science* **115**:4925–4936. DOI: https://doi.org/10.1242/jcs.00181, PMID: 12432079

Lansman JB, Hess P, Tsien RW. 1986. Blockade of current through single calcium channels by Cd^{2+}, Mg^{2+}, and Ca^{2+}. voltage and concentration dependence of calcium entry into the pore. *The Journal of General Physiology* **88**:321–347. DOI: https://doi.org/10.1085/jgp.88.3.321, PMID: 2428920

Lee SH, Ho WK, Lee SH. 2009. Characterization of somatic Ca^{2+} clearance mechanisms in young and mature hippocampal granule cells. *Cell Calcium* **45**:465–473. DOI: https://doi.org/10.1016/j.ceca.2009.03.004, PMID: 19362367

Lee SH, Kim KR, Ryu SY, Son S, Hong HS, Mook-Jung I, Lee SH, Ho WK. 2012. Impaired short-term plasticity in mossy fiber synapses caused by mitochondrial dysfunction of dentate granule cells is the earliest synaptic deficit in a mouse model of Alzheimer's disease. *The Journal of Neuroscience* **32**:5953–5963. DOI: https://doi.org/10.1523/JNEUROSCI.0465-12.2012, PMID: 22539855

Lee SY, Vuong TA, Wen X, Jeong HJ, So HK, Kwon I, Kang JS, Cho H. 2019. Methylation determines the extracellular calcium sensitivity of the leak channel NALCN in hippocampal dentate granule cells. *Experimental & Molecular Medicine* **51**:1–14. DOI: https://doi.org/10.1038/s12276-019-0325-0, PMID: 31601786

Lennie P. 2003. The cost of cortical computation. *Current Biology* **13**:493–497. DOI: https://doi.org/10.1016/s0960-9822(03)00135-0, PMID: 12646132

Liesegang GW, Farrow MM, Arce Vazquez F, Purdie N, Eyring EM. 1977. Ultrasonic absorption kinetic studies of the complexation of aqueous Li^+, Na^+, Rb^+, Tl^+, Ag^+, NH_4^+, and Ca^{2+} by 18-crown-6. *Journal of the American Chemical Society* **99**:3240–3243. DOI: https://doi.org/10.1021/ja00452a006

Lipton P, Robacker K. 1983. Glycolysis and brain function: $[K^+]$ o stimulation of protein synthesis and K^+ uptake require glycolysis. *Federation Proceedings* **42**:2875–2880 PMID: 6136420.

Lu B, Zhang Q, Wang H, Wang Y, Nakayama M, Ren D. 2010. Extracellular calcium controls background current and neuronal excitability via an UNC79-UNC80-NALCN cation channel complex. *Neuron* **68**:488–499. DOI: https://doi.org/10.1016/j.neuron.2010.09.014, PMID: 21040849

Lynch RM, Balaban RS. 1987. Coupling of aerobic glycolysis and Na^+-K^+-ATPase in renal cell line MDCK. *The American Journal of Physiology* **253**:C269–C276. DOI: https://doi.org/10.1152/ajpcell.1987.253.2.C269, PMID: 3039854

Marks MJ, Seeds NW. 1978. A heterogeneous ouabain-ATPase interaction in mouse brain. *Life Sciences* **23**:2735–2744. DOI: https://doi.org/10.1016/0024-3205(78)90654-9, PMID: 216868

McKenna MC, Waagepetersen HS, Schousboe A, Sonnewald U. 2006. Neuronal and astrocytic shuttle mechanisms for cytosolic-mitochondrial transfer of reducing equivalents: current evidence and pharmacological tools. *Biochemical Pharmacology* **71**:399–407. DOI: https://doi.org/10.1016/j.bcp.2005.10.011, PMID: 16368075

Meier SD, Kovalchuk Y, Rose CR. 2006. Properties of the new fluorescent Na^+ indicator corona green: comparison with SBFI and confocal Na^+ imaging. *Journal of Neuroscience Methods* **155**:251–259. DOI: https://doi.org/10.1016/j.jneumeth.2006.01.009, PMID: 16488020

Mercer RW, Dunham PB. 1981. Membrane-bound ATP fuels the Na/K pump. Studies on membrane-bound glycolytic enzymes on inside-out vesicles from human red cell membranes. *The Journal of General Physiology* **78**:547–568. DOI: https://doi.org/10.1085/jgp.78.5.547, PMID: 6273495

Meyer DJ, Gatto C, Artigas P. 2017. On the effect of hyperaldosteronism-inducing mutations in Na/K pumps. *Journal of General Physiology* **149**:1009–1028. DOI: https://doi.org/10.1085/jgp.201711827

Meyer DJ, Gatto C, Artigas P. 2019. Na/K pump mutations associated with primary hyperaldosteronism cause loss of function. *Biochemistry* **58**:1774–1785. DOI: https://doi.org/10.1021/acs.biochem.9b00051, PMID: 30811176

Meyer DJ, Bijlani S, de Sautu M, Spontarelli K, Young VC, Gatto C, Artigas P. 2020. FXYD protein isoforms differentially modulate human Na/K pump function. *Journal of General Physiology* **152**:e202012660. DOI: https://doi.org/10.1085/jgp.202012660

Milligan LP, McBride BW. 1985. Energy costs of ion pumping by animal tissues. *The Journal of Nutrition* **115**:1374–1382. DOI: https://doi.org/10.1093/jn/115.10.1374, PMID: 2413191

Minakami S, Kakinuma K, Yoshikawa H. 1964. The control of erythrocyte glycolysis by active cation transport. *Biochimica et Biophysica Acta (BBA) - General Subjects* **90**:434–436. DOI: https://doi.org/10.1016/0304-4165(64)90219-3

Miura Y, Kimura J. 1989. Sodium-calcium exchange current. Dependence on internal Ca and Na and competitive binding of external Na and Ca. *The Journal of General Physiology* **93**:1129–1145. DOI: https://doi.org/10.1085/jgp.93.6.1129, PMID: 2549177

Mohler PJ, Davis JQ, Bennett V. 2005. Ankyrin-B coordinates the Na/K ATPase, Na/Ca exchanger, and $InsP_3$ receptor in a cardiac T-tubule/SR microdomain. *PLOS Biology* **3**:e423. DOI: https://doi.org/10.1371/journal.pbio.0030423, PMID: 16292983

Mondragão MA, Schmidt H, Kleinhans C, Langer J, Kafitz KW, Rose CR. 2016. Extrusion versus diffusion: mechanisms for recovery from sodium loads in mouse CA1 pyramidal neurons. *The Journal of Physiology* **594**:5507–5527. DOI: https://doi.org/10.1113/JP272431, PMID: 27080107

Mongeon R, Venkatachalam V, Yellen G. 2016. Cytosolic NADH-NAD^+ redox visualized in brain slices by two-photon fluorescence lifetime biosensor imaging. *Antioxidants & Redox Signaling* **25**:553–563. DOI: https://doi.org/10.1089/ars.2015.6593, PMID: 26857245

Nelson DL, Lehninger AL, Cox MM. 2008. Lehninger Principles of Biochemistry. Macmillan.

Nevian T, Helmchen F. 2007. Calcium indicator loading of neurons using single-cell electroporation. *Pflugers Archiv* **454**:675–688. DOI: https://doi.org/10.1007/s00424-007-0234-2, PMID: 17334778

Niggli V, Sigel E, Carafoli E. 1982. The purified Ca^{2+} pump of human erythrocyte membranes catalyzes an electroneutral Ca^{2+}-H^+ exchange in reconstituted liposomal systems. *The Journal of Biological Chemistry* **257**:2350–2356. DOI: https://doi.org/10.1016/S0021-9258(18)34929-9, PMID: 6460758

Ovádi J, Saks V. 2004. On the origin of intracellular compartmentation and organized metabolic systems. *Molecular and Cellular Biochemistry* **256–257**:5–12. DOI: https://doi.org/10.1023/b:mcbi.0000009855.14648.2c, PMID: 14977166

Palty R, Sekler I. 2012. The mitochondrial Na^+/Ca^{2+} exchanger. *Cell Calcium* **52**:9–15. DOI: https://doi.org/10.1016/j.ceca.2012.02.010, PMID: 22430014

Parpura V, Sekler I, Fern R. 2016. Plasmalemmal and mitochondrial Na^+-Ca^{2+} exchange in neuroglia. *Glia* **64**:1646–1654. DOI: https://doi.org/10.1002/glia.22975, PMID: 27143128

Paul RJ, Bauer M, Pease W. 1979. Vascular smooth muscle: aerobic glycolysis linked to sodium and potassium transport processes. *Science* **206**:1414–1416. DOI: https://doi.org/10.1126/science.505014, PMID: 505014

Paul RJ. 1983. Functional compartmentalization of oxidative and glycolytic metabolism in vascular smooth muscle. *American Journal of Physiology-Cell Physiology* **244**:C399–C409. DOI: https://doi.org/10.1152/ajpcell.1983.244.5.C399

Pologruto TA, Sabatini BL, Svoboda K. 2003. ScanImage: flexible software for operating laser scanning microscopes. *BioMedical Engineering OnLine* **2**:13. DOI: https://doi.org/10.1186/1475-925X-2-13

Post RL, Sen AK, Rosenthal AS. 1965. A phosphorylated intermediate in adenosine triphosphate-dependent sodium and potassium transport across kidney membranes. *The Journal of Biological Chemistry* **240**:1437–1445 PMID: 14284759.

Proverbio F, Hoffman JF. 1977. Membrane compartmentalized ATP and its preferential use by the Na,K-ATPase of human red cell ghosts. *The Journal of General Physiology* **69**:605–632. DOI: https://doi.org/10.1085/jgp.69.5.605, PMID: 140926

Pusch M, Neher E. 1988. Rates of diffusional exchange between small cells and a measuring patch pipette. *Pflugers Archiv* **411**:204–211. DOI: https://doi.org/10.1007/BF00582316, PMID: 2451806

Rolfe DF, Brown GC. 1997. Cellular energy utilization and molecular origin of standard metabolic rate in mammals. *Physiological Reviews* **77**:731–758. DOI: https://doi.org/10.1152/physrev.1997.77.3.731, PMID: 9234964

Rose CR, Kovalchuk Y, Eilers J, Konnerth A. 1999. Two-photon Na^+ imaging in spines and fine dendrites of central neurons. *Pflugers Archiv* **439**:201–207. DOI: https://doi.org/10.1007/s004249900123, PMID: 10651018

San Martín A, Ceballo S, Ruminot I, Lerchundi R, Frommer WB, Barros LF. 2013. A genetically encoded FRET lactate sensor and its use to detect the warburg effect in single cancer cells. *PLOS ONE* **8**:e57712. DOI: https://doi.org/10.1371/journal.pone.0057712, PMID: 23469056

San Martín A, Ceballo S, Baeza-Lehnert F, Lerchundi R, Valdebenito R, Contreras-Baeza Y, Alegría K, Barros LF. 2014. Imaging mitochondrial flux in single cells with a FRET sensor for pyruvate. *PLOS ONE* **9**:e85780. DOI: https://doi.org/10.1371/journal.pone.0085780, PMID: 24465702

Saotome M, Katoh H, Satoh H, Nagasaka S, Yoshihara S, Terada H, Hayashi H. 2005. Mitochondrial membrane potential modulates regulation of mitochondrial Ca^{2+} in rat ventricular myocytes. *American Journal of Physiology. Heart and Circulatory Physiology* **288**:H1820–H1828. DOI: https://doi.org/10.1152/ajpheart.00589.2004, PMID: 15563537

Satrústegui J, Bak LK. 2015. Fluctuations in cytosolic calcium regulate the neuronal malate-aspartate NADH shuttle: implications for neuronal energy metabolism. *Neurochemical Research* **40**:2425–2430. DOI: https://doi.org/10.1007/s11064-015-1652-8, PMID: 26138554

Schöneberg T, Kloos M, Brüser A, Kirchberger J, Sträter N. 2013. Structure and allosteric regulation of eukaryotic 6-phosphofructokinases. *Biological Chemistry* **394**:977–993. DOI: https://doi.org/10.1515/hsz-2013-0130, PMID: 23729568

Secondo A, Pignataro G, Ambrosino P, Pannaccione A, Molinaro P, Boscia F, Cantile M, Cuomo O, Esposito A, Sisalli MJ, Scorziello A, Guida N, Anzilotti S, Fiorino F, Severino B, Santagada V, Caliendo G, Di Renzo G, Annunziato L. 2015. Pharmacological characterization of the newly synthesized 5-amino-*N*-butyl-2-(4-ethoxyphenoxy)-benzamide hydrochloride (BED) as a potent NCX3 inhibitor that worsens anoxic injury in cortical neurons, organotypic hippocampal cultures, and ischemic brain. *ACS Chemical Neuroscience* **6**:1361–1370. DOI: https://doi.org/10.1021/acschemneuro.5b00043, PMID: 25942323

Sen AK, Post RL. 1964. Stoichiometry and localization of adenosine triphosphate-dependent sodium and potassium transport in the erythrocyte. *Journal of Biological Chemistry* **239**:345–352. DOI: https://doi.org/10.1016/S0021-9258(18)51788-9

Sharikabad MN, Cragoe EJ, Brørs O. 1997. Inhibition by 5-N-(4-chlorobenzyl)-2′,4′-dimethylbenzamil of Na^+/Ca^{2+} exchange and L-type Ca^{2+} channels in isolated cardiomyocytes. *Pharmacology & Toxicology* **80**:57–61. DOI: https://doi.org/10.1111/j.1600-0773.1997.tb00284.x, PMID: 9060035

Spohr L, Soares MSP, Bona NP, Pedra NS, Barschak AG, Alvariz RM, Vizzotto M, Lencina CL, Stefanello FM, Spanevello RM. 2022. Effect of blueberry extract on energetic metabolism, levels of brain-derived neurotrophic factor, and Ca^{2+}-ATPase activity in the hippocampus and cerebral cortex of rats submitted to ketamine-induced mania-like behavior. *Metabolic Brain Disease* **37**:835–847. DOI: https://doi.org/10.1007/s11011-022-00904-x, PMID: 35043268

Sweadner KJ. 1979. Two molecular forms of (Na^+ + K^+) -stimulated ATPase in brain. Separation, and difference in affinity for strophanthidin. *The Journal of Biological Chemistry* **254**:6060–6067 PMID: 221488.

Tantama M, Martínez-François JR, Mongeon R, Yellen G. 2013. Imaging energy status in live cells with a fluorescent biosensor of the intracellular ATP-to-ADP ratio. *Nature Communications* **4**:2550. DOI: https://doi.org/10.1038/ncomms3550, PMID: 24096541

Teixeira FC, Gutierres JM, Soares MSP, da Siveira de Mattos B, Spohr L, do Couto CAT, Bona NP, Assmann CE, Morsch VM, da Cruz IBM, Stefanello FM, Spanevello RM. 2020. Inosine protects against impairment of memory induced by experimental model of Alzheimer disease: a nucleoside with multitarget brain actions. *Psychopharmacology* **237**:811–823. DOI: https://doi.org/10.1007/s00213-019-05419-5, PMID: 31834453

Thomas RC. 2009. The plasma membrane calcium ATPase (PMCA) of neurones is electroneutral and exchanges 2 H^+ for each Ca^{2+} or Ba^{2+} ion extruded. *The Journal of Physiology* **587**:315–327. DOI: https://doi.org/10.1113/jphysiol.2008.162453, PMID: 19064619

Tomokuni Y, Goryo K, Katsura A, Torii S, Yasumoto K, Kemnitz K, Takada M, Fukumura H, Sogawa K. 2010. Loose interaction between glyceraldehyde-3-phosphate dehydrogenase and phosphoglycerate kinase revealed by fluorescence resonance energy transfer-fluorescence lifetime imaging microscopy in living cells. *The FEBS Journal* **277**:1310–1318. DOI: https://doi.org/10.1111/j.1742-4658.2010.07561.x, PMID: 20392205

Tran K, Smith NP, Loiselle DS, Crampin EJ. 2009. A thermodynamic model of the cardiac sarcoplasmic/endoplasmic Ca^{2+} (SERCA) pump. *Biophysical Journal* **96**:2029–2042. DOI: https://doi.org/10.1016/j.bpj.2008.11.045, PMID: 19254563

Tsien RW, Hess P, McCleskey EW, Rosenberg RL. 1987. Calcium channels: mechanisms of selectivity, permeation, and block. *Annual Review of Biophysics and Biophysical Chemistry* **16**:265–290. DOI: https://doi.org/10.1146/annurev.bb.16.060187.001405, PMID: 2439098

Wallimann T, Wyss M, Brdiczka D, Nicolay K, Eppenberger HM. 1992. Intracellular compartmentation, structure and function of creatine kinase isoenzymes in tissues with high and fluctuating energy demands: the 'phosphocreatine circuit' for cellular energy homeostasis. *The Biochemical Journal* **281 (Pt 1)**:21–40. DOI: https://doi.org/10.1042/bj2810021, PMID: 1731757

Weiss J, Hiltbrand B. 1985. Functional compartmentation of glycolytic versus oxidative metabolism in isolated rabbit heart. *The Journal of Clinical Investigation* **75**:436–447. DOI: https://doi.org/10.1172/JCI111718, PMID: 3973013

Whittam R. 1962. The dependence of the respiration of brain cortex on active cation transport. *The Biochemical Journal* **82**:205–212. DOI: https://doi.org/10.1042/bj0820205, PMID: 14006661

Whittam R, Ager ME, Wiley JS. 1964. Control of lactate production by membrane adenosine triphosphatase activity in human erythrocytes. *Nature* **202**:1111–1112. DOI: https://doi.org/10.1038/2021111a0, PMID: 14207205

Whittam R, Ager ME. 1965. The connexion between active cation transport and metabolism in erythrocytes. *The Biochemical Journal* **97**:214–227. DOI: https://doi.org/10.1042/bj0970214, PMID: 16749106

Xu KY, Zweier JL, Becker LC. 1995. Functional coupling between glycolysis and sarcoplasmic reticulum Ca^{2+} transport. *Circulation Research* **77**:88–97. DOI: https://doi.org/10.1161/01.res.77.1.88, PMID: 7788886

Yasuda R, Harvey CD, Zhong H, Sobczyk A, van Aelst L, Svoboda K. 2006. Supersensitive ras activation in dendrites and spines revealed by two-photon fluorescence lifetime imaging. *Nature Neuroscience* **9**:283–291. DOI: https://doi.org/10.1038/nn1635, PMID: 16429133

Yu Y, Herman P, Rothman DL, Agarwal D, Hyder F. 2018. Evaluating the gray and white matter energy budgets of human brain function. *Journal of Cerebral Blood Flow and Metabolism* **38**:1339–1353. DOI: https://doi.org/10.1177/0271678X17708691, PMID: 28589753

Zhang XQ, Wang J, Carl LL, Song J, Ahlers BA, Cheung JY. 2009. Phospholemman regulates cardiac Na^+/Ca^{2+} exchanger by interacting with the exchanger's proximal linker domain. *American Journal of Physiology. Cell Physiology* **296**:C911–C921. DOI: https://doi.org/10.1152/ajpcell.00196.2008, PMID: 19158404

Zhang XQ, Wang J, Song J, Ji AM, Chan TO, Cheung JY. 2011. Residues 248-252 and 300-304 of the cardiac Na^+/Ca^{2+} exchanger are involved in its regulation by phospholemman. *American Journal of Physiology. Cell Physiology* **301**:C833–C840. DOI: https://doi.org/10.1152/ajpcell.00069.2011, PMID: 21734189